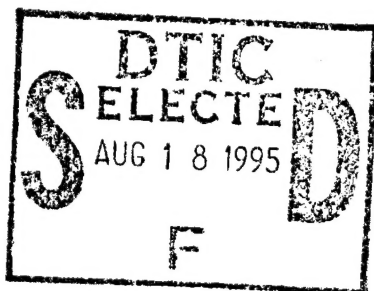# NAVAL POSTGRADUATE SCHOOL
MONTEREY, CALIFORNIA

THESIS

RADIOWAVE PROPAGATION OVER AN
IRREGULAR TERRAIN USING THE
PARABOLIC EQUATION METHOD IN A
CURVILINEAR COORDINATE SYSTEM

by

Lee, Joo-Kiong

March, 1995

Thesis Advisor: Ramakrishna Janaswamy

Approved for public release; distribution is unlimited.

REPORT DOCUMENTATION PAGE

Form Approved OMB No. 0704-0188

1. AGENCY USE ONLY *(Leave blank)*	2. REPORT DATE March 1995	3. REPORT TYPE AND DATES COVERED Master's Thesis	
4. TITLE AND SUBTITLE RADIOWAVE PROPAGATION OVER AN IRREGULAR TERRAIN USING THE PARABOLIC EQUATION METHOD IN A CURVILINEAR COORDINATE SYSTEM		5. FUNDING NUMBERS	
6. AUTHOR(S) Lee, Joo-Kiong			
7. PERFORMING ORGANIZATION NAME(S) AND ADDRESS(ES) Naval Postgraduate School Monterey CA 93943-5000		8. PERFORMING ORGANIZATION REPORT NUMBER	
9. SPONSORING/MONITORING AGENCY NAME(S) AND ADDRESS(ES)		10. SPONSORING/MONITORING AGENCY REPORT NUMBER	

11. SUPPLEMENTARY NOTES The views expressed in this thesis are those of the author and do not reflect the official policy or position of the Department of Defense or the U.S. Government.

12a. DISTRIBUTION/AVAILABILITY STATEMENT Approved for public release; distribution is unlimited.	12b. DISTRIBUTION CODE

13. ABSTRACT *(maximum 200 words)*

The problem of radiowave propagation over irregular terrain is solved by using the standard parabolic equation method. The ground is characterized by an impedance boundary condition and a height profile. A tropospheric boundary condition is used to truncate the computational domain. This thesis uses a novel approach of casting all the equations in a curvilinear coordinate system. The coordinate system is generated in a simple manner using the ground profile data. The equations are solved by the finite difference method using the Crank-Nicolson scheme. Different numerical values for various important parameters (e.g., step size, location of tropospheric boundary, the region above the tropospheric boundary, etc.) were used, and their effect on the accuracy and computing time are discussed. Validation of the numerical results with exact and/or experimental results are presented for different terrain profiles. Both perfectly electric conducting (PEC) and lossy impedance surfaces are considered.

14. SUBJECT TERMS Propagation, Parabolic Equation, Curvilinear Coordinate System			15. NUMBER OF PAGES 101
			16. PRICE CODE
17. SECURITY CLASSIFICATION OF REPORT Unclassified	18. SECURITY CLASSIFICATION OF THIS PAGE Unclassified	19. SECURITY CLASSIFICATION OF ABSTRACT Unclassified	20. LIMITATION OF ABSTRACT UL

NSN 7540-01-280-5500

Standard Form 298 (Rev. 2-89)
Prescribed by ANSI Std. 239-18 298-102

RADIOWAVE PROPAGATION OVER AN IRREGULAR TERRAIN USING THE PARABOLIC EQUATION METHOD IN A CURVILINEAR COORDINATE SYSTEM

by

Lee, Joo-Kiong
Major, Singapore Air Force
B.S.E.E., Nanyang Technological Institute, Singapore, 1985

Submitted in partial fulfillment
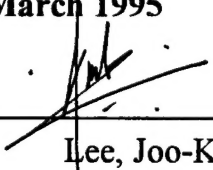of the requirements for the degree of

MASTER OF SCIENCE IN ELECTRICAL ENGINEERING

from the

NAVAL POSTGRADUATE SCHOOL
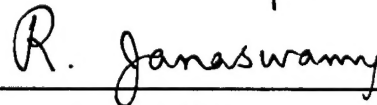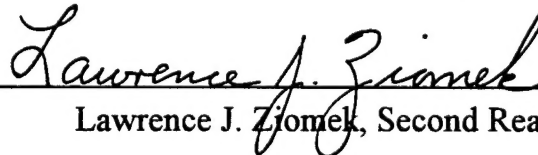### March 1995

Author: _____
Lee, Joo-Kiong

Approved by: _____
Ramakrishna Janaswamy, Thesis Advisor

_____
Lawrence J. Ziomek, Second Reader

_____
Michael A. Morgan, Chairman
Department of Electrical and Computer Engineering

iii

ABSTRACT

The problem of radiowave propagation over irregular terrain is solved by using the standard parabolic equation method. The ground is characterized by an impedance boundary condition and a height profile. A tropospheric boundary condition is used to truncate the computational domain. This thesis uses a novel approach of casting all the equations in a curvilinear coordinate system. The coordinate system is generated in a simple manner using the ground profile data. The equations are solved by the finite difference method using the Crank-Nicolson scheme.

Different numerical values for various important parameters (e.g., step size, location of tropospheric boundary, the region above the tropospheric boundary, etc.) were used, and their effect on the accuracy and computing time are discussed. Validation of the numerical results with exact and/or experimental results are presented for different terrain profiles. Both perfectly electric conducting (PEC) and lossy impedance surfaces are considered.

Accesion For		
NTIS CRA&I	☑	
DTIC TAB	☐	
Unannounced	☐	
Justification		
By		
Distribution /		
Availability Codes		
Dist	Avail and / or Special	
A-1		

TABLE OF CONTENTS

LIST OF TABLES

LIST OF FIGURES

I. INTRODUCTION

A. BACKGROUND

The topic of radiowave propagation over irregular terrain is extremely important in ground-to-ground as well as in ground-to-air communications used by the Navy, Air Force, and the Army. Similarly, the ability to predict radiowave propagation over irregular terrain has a significant impact in determining target detectability in a radar system. The physics of propagation is affected by ever-changing atmospheric conditions and by complex terrain features on the ground. The link reliability in a communication system or target detectability in radar can be significantly affected by the so called 'multipath fading'. The path between a transmitter and a receiver is often obstructed by natural or man-made obstacles such as hills, buildings, atmospheric layers, trees, rain, fog, etc. In the case of atmospheric multipath fading, abnormal propagation of electromagnetic waves resulting from super-refraction or sub-refraction can result in severe loss of signals. Reflection multipath fading, which is due to interference between the direct and the ground reflected waves depends strongly on the terrain geometry and ground constants. It is therefore important to designers and operators of communications and radar systems to predict the electromagnetic fields due to radiating sources in the troposphere and to assess the effects of environment on radiowave propagation.

Any in-depth understanding of these systems requires a knowledge of the physical phenomena that governs low-angle propagation; more specifically, to be able to model complex fading phenomena due to refraction, reflection, scattering, and diffraction. Numerous analytical methods are available for predicting electromagnetic wave propagation such as geometric optics, physical optics, normal mode analysis, and combinations of the above. However, they have several limitations for predicting propagation in a complex environment. The parabolic equation method has been used to predict radiowave propagation in an inhomogeneous atmosphere and over flat terrain, and also for predicting radiowave propagation over sloping irregularities.

1

In this thesis, we will concentrate solely on the effects of irregular terrain. Since the propagation path could extend over several thousands of wavelengths, it is important to have a method that is efficient numerically. The parabolic equation method is one such method. One advantage of a parabolic partial differential equation (PDE) over an elliptic PDE is that in the former case, the field at any location can be computed in terms of the field at a previous location. However, this would be accurate only when the waves propagate predominantly in the forward direction. In deriving a parabolic PDE, it is assumed that the waves are predominantly forward traveling. This is approximately met in a typical radio link where the received signal is primarily affected by the nature of the path between the transmitting and receiving antennas. Of course there are several situations when this is not true. For example, when there is a large obstacle behind a receiving antenna, back-scattering from the obstacle will affect the received signal. Nonetheless, the parabolic equation method has been used successfully in the past to predict propagation in several scenarios, particularly for atmospheric multipath fading.

B.   OBJECTIVE

In this thesis, we adopt the same parabolic PDE as in the previous approach [Ref. 1] to predict radiowave propagation over an irregular terrain. A tropospheric boundary condition is used to truncate the computational domain at the top, while an impedance boundary condition is used on the uneven terrain to characterize the ground. The key feature of this thesis is to use a novel approach of casting all the equations in a curvilinear coordinate system. A body fitted coordinate system is generated based on the specification of the ground profile. This permits accurate modeling of the boundary conditions which is so vital to the success of the model. The parabolic equation method is a full-wave method in that it includes all aspects of wave propagation such as forward reflection, refraction, diffraction, and surface wave propagation. However, as stated above, it ignores back-scattering. Chapter II presents the derivation and formulation of the governing partial differential equation for the standard parabolic equation method, the impedance boundary condition, and the tropospheric boundary condition. Also presented in Chapter II is the transformation of all the partial differential

2

equations to a curvilinear coordinate system. Chapter III details the generation of the coordinate system and the numerical procedure for solving the parabolic PDE. The performance of the numerical solution is examined in Chapter IV. This includes a study on the effects of using different numerical values for various important parameters (e.g., step size, location of the tropospheric boundary, the region above the tropospheric boundary, etc.) on the accuracy of the solution, and validation of the numerical results with exact and/or experimental results for different terrain profiles. Recommendations and conclusions are presented in Chapter V. Finally, MATLAB computer codes for the numerical implementation are presented in the Appendix.

II. FORMULATION

In this chapter we present the governing partial differential equation for the fields together with the required boundary conditions. We present only the final forms and refer the reader to [Ref. 2] for more details. Figure 1 shows a Hertzian electric source placed over an irregular, lossy terrain. The terrain is characterized by its height profile and an impedance boundary condition. The impedance of the ground depends on the ground constants ($\epsilon_o \epsilon_r$, $\mu_o \mu_r$, and σ). We wish to solve the fields at a point on/over the ground in the presence of the irregularities. We consider only a 2-dimensional situation where the sources, geometry, and all fields are z-invariant.
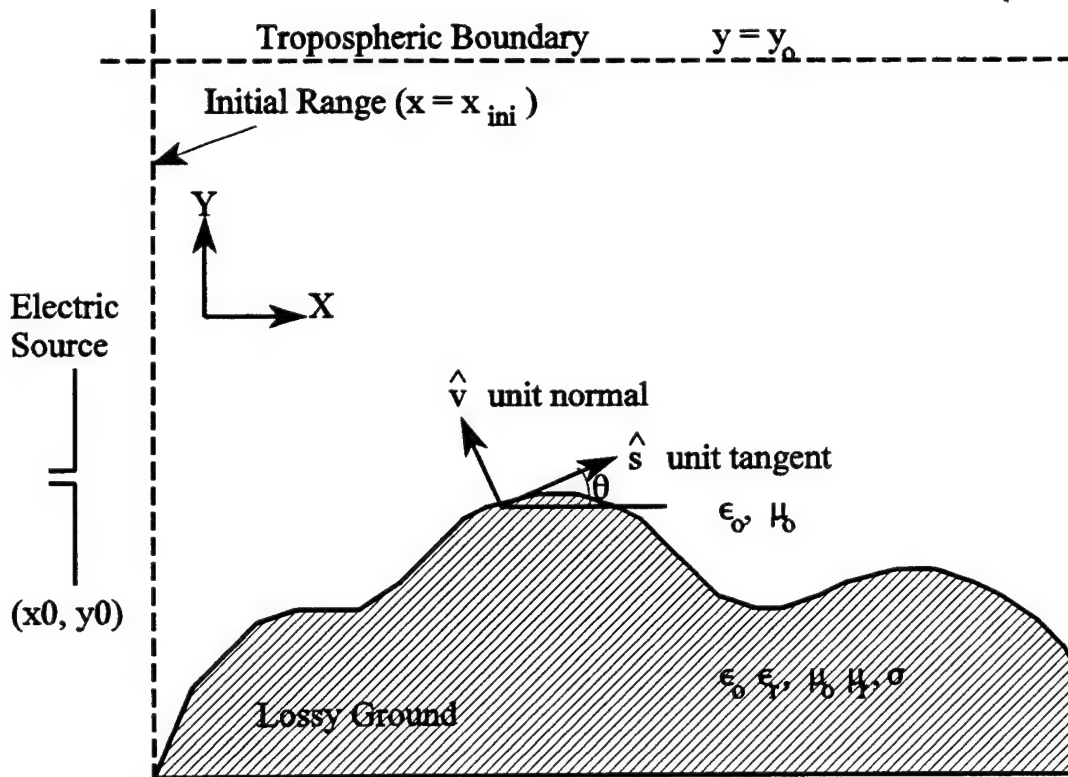
Figure 1.   An electric source producing fields over an irregular terrain.

Section A deals with the impedance boundary condition. In Section B, we present the theory on the parabolic PDE. In Section C, we present the tropospheric boundary condition required to terminate the computational domain. In any partial differential equation, proper imposition of boundary conditions is very critical to the final solution. We desire to solve the parabolic PDE by an implicit finite difference scheme. Most of the previous work in this area used a cartesian mesh because of its simplicity. However, practical geometries seldom conform to cartesian coordinates. Some sort of interpolation is needed near the boundary when non-cartesian geometries are encountered, as in the present case. This could result in a severe loss of accuracy. To better model the boundary conditions, we solve the equations in a curvilinear coordinate system generated by treating the lower irregular boundary as one coordinate line. In Section D, we cast all the equations in a curvilinear coordinate system.

A.   IMPEDANCE BOUNDARY CONDITION

An impedance boundary condition (IBC) relates the tangential components of the electric and magnetic fields at the interface of two media. If $\hat{v}$ is a unit normal vector to the boundary, and $\hat{s}$ is a unit tangential vector as shown in Fig. 1, the boundary condition is [Ref. 3]

$$\hat{v} \times (\hat{v} \times \vec{E}) = -\eta_o \Delta_s \hat{v} \times \vec{H}, \tag{1}$$

where $\Delta_s = Z_s/\eta_o$ is the surface impedance normalized to the free-space impedance $\eta_o = \sqrt{\mu_o/\epsilon_o}$ and Z_s is the actual surface impedance that is dependent on the media constants and the incident angles. The surface impedance is determined from the intrinsic impedance of the medium by considering plane wave reflections from the interface. Figure 2 shows the interface between two media. The complex propagation constants, γ_1, γ_2, and the intrinsic impedances η_1 and η_2 can be expressed in terms of the media constants. They are

$$\gamma_1^2 = j\omega\mu_o(j\omega\epsilon_o) = -k_o^2, \tag{2}$$

$$\gamma_2^2 = j\omega\mu_r\mu_o(\sigma + j\omega\epsilon_o\epsilon_r) = -k_o^2\mu_r\epsilon_{rc}, \tag{3}$$

6
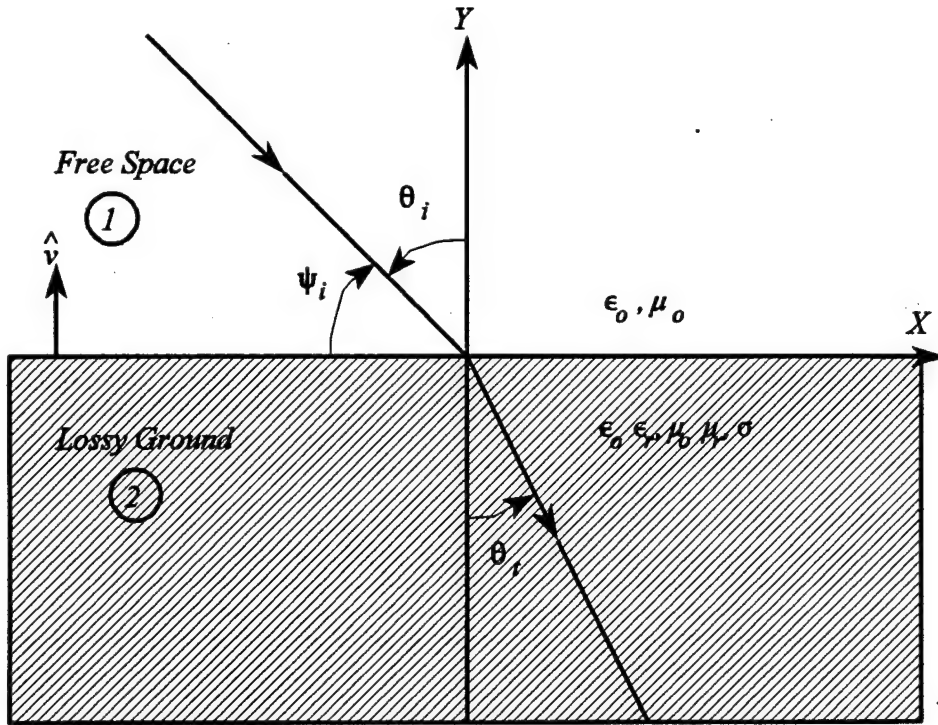
Figure 2.   Boundary interface between two regions.

and

$$\eta_1 = \eta_o, \qquad \eta_2 = \eta_o \sqrt{\frac{\mu_{r2}}{\epsilon_{rc2}}} . \tag{4}$$

According to Snell's law, $\gamma_1 \sin \theta_i = \gamma_2 \sin \theta_t$. The plane-wave reflection coefficients for the vertical and horizontal polarizations, R_V and R_H, are [Ref. 4]

$$R_H = \frac{\eta_2 \sec \theta_t - \eta_0 \sec \theta_i}{\eta_2 \sec \theta_t + \eta_0 \sec \theta_i} , \tag{5}$$

$$R_V = \frac{\eta_2 \cos \theta_t - \eta_1 \cos \theta_i}{\eta_2 \cos \theta_t + \eta_1 \cos \theta_i} . \tag{6}$$

Using these, the surface impedance of the lossy ground can be taken as

7

$$Z_s = \begin{cases} Z_s^H = \eta_2 \sec\theta_{t'} & \text{Horizontal Polarization} \\ Z_s^V = \eta_2 \cos\theta_{t'} & \text{Vertical Polarization} \end{cases} \tag{7}$$

Therefore,

$$\Delta_s^H = \sqrt{\frac{\mu_r}{\epsilon_{rc}}} \cdot \left[1 - \frac{\cos^2\psi_i}{\mu_r \epsilon_{rc}} \right]^{\frac{1}{2}}, \quad \Delta_s^V = \sqrt{\frac{\mu_r}{\epsilon_{rc}}} \cdot \left[1 - \frac{\cos^2\psi_i}{\mu_r \epsilon_{rc}} \right]^{\frac{1}{2}}. \tag{8}$$

For the special case of normal incidence, $\psi_i = 90°$,

$$\Delta_s^H = \Delta_s^V = \sqrt{\frac{1}{\epsilon_r - j\sigma_r}}, \tag{9}$$

where $\sigma_r = \dfrac{\sigma}{\omega\epsilon_o}$. In this thesis, we will use a normalized surface impedance given in Eq. (9) for all the results. For a 2-Dimensional case with vertical polarization, the impedance boundary condition given by Eq. (1) can be simplified as

$$\frac{\partial H_z}{\partial v} - jk_o \epsilon_r \Delta_s^V H_z = 0. \qquad \text{IBC Vertical Polarization} \tag{10}$$

Similarly, we have for the horizontal polarization

$$\frac{\partial E_z}{\partial v} - jk_o \mu_r \frac{1}{\Delta_s^H} E_z = 0. \qquad \text{IBC Horizontal Polarization} \tag{11}$$

For a perfectly conducting material, $\Delta_s^{H/V} = 0$ and the impedance boundary condition reduces to $\dfrac{\partial H_z}{\partial v} = 0$ (Vertical Polarization) and $E_z = 0$ (Horizontal Polarization).

B.   STANDARD PARABOLIC PARTIAL DIFFERENTIAL EQUATION

For a two-dimensional electric source producing fields in a homogeneous region, all quantities are independent of the z-coordinate, and propagation takes place in the xy-plane. From Maxwell's equations, we have $\nabla \times \vec{E} = -j\omega\mu\vec{H}$, and $\nabla \times \vec{H} = j\omega\epsilon\vec{E} + \vec{J}$. The fields could be expressed in terms of the z-component of the magnetic field, H_z, in the case of vertical polarization (TE_z fields), and in terms of E_z for the horizontal polarization (TM_z

8

fields). In a source-free environment, the equation satisfied by the magnetic field is

$$\nabla \cdot (\nabla H_z) + k_o^2 H_z = 0. \qquad \text{Vertical Polarization} \qquad (12)$$

Similarly the equation for the electric field is

$$\nabla \cdot (\nabla E_z) + k_o^2 E_z = 0. \qquad \text{Horizontal Polarization} \qquad (13)$$

Equations (12) and (13) may be combined into an equation of the form

$$\nabla^2 \psi + k_o^2 \psi = 0, \qquad (14)$$

where $\psi = H_z$ for TE Polarization and $\psi = E_z$ for TM Polarization. Equation (14) is the standard Helmholtz equation and is elliptic in nature; the field at any one point depends on field at every other point in a complicated manner. However, for wave propagation problems, an approximate answer can be obtained by the use of a parabolic PDE. In this case, the field at a particular range depends on the field at previous range points only. Assuming that the wave propagates predominantly in the positive x-direction, we write

$$\psi(x,y) = e^{-jk_o x} u(x,y), \qquad (15)$$

where $u(x,y)$ is a slowly varying function of x. We now impose the restriction that

$$|u_{xx}| \ll 2k_o |u_x| \qquad (16)$$

$(u_x = \dfrac{\partial u}{\partial x} , u_{xx} = \dfrac{\partial^2 u}{\partial x^2})$ into Eq. (14) and arrive at

$$\frac{\partial u}{\partial x} = \frac{-j}{2k_o} \frac{\partial^2 u}{\partial y^2} . \qquad (17)$$

Equation (17) is the exact form of the narrow angle parabolic PDE approximation. The impedance boundary conditions derived in the previous section can also be expressed in terms of the 'u' function :

$$u_y - jk_o(\Delta_s^\gamma + x_y)u = 0, \qquad \text{IBC Vertical Polarization} \qquad (18)$$

9

$$u_v - jk_o\left(\frac{1}{\Delta_s^H} + x_v\right)u = 0, \qquad \text{IBC Horizontal Polarization} \tag{19}$$

where $x_v = \dfrac{\partial x}{\partial v} = -\sin\theta$ and $u_v = \dfrac{\partial u}{\partial v}$ on the irregular terrain. By defining

$$c_1 = \begin{cases} -jk_o(\Delta_s^V - \sin\theta) & \text{Vertical Polarization} \\ -jk_o(\dfrac{1}{\Delta_s^H} - \sin\theta) & \text{Horizontal Polarization} \end{cases}, \tag{20}$$

Eqs. (18) and (19) can be combined and written as

$$u_v + c_1 u = 0. \tag{21}$$

The parabolic PDE given by Eq. (17) is valid for propagation angles close to the horizontal ($\pm 15°$ in practice) [Ref. 5].

C. TROPOSPHERIC BOUNDARY CONDITION

Our computational domain consists of the region above the lossy ground. To truncate the computational domain on the upper side, we consider a point $y = y_o$ high enough and impose a boundary condition of the form

$$u_y + \alpha u = \beta \qquad \text{on } y = y_o. \tag{22}$$

To derive this, we start with the parabolic equation $u_{yy} - 2jku_x = 0$ with a complex k. Consider the problem of determining the field at any point in $x > x_{ini}$ and $y > y_o$, given the initial data on $x = x_{ini}$, $u(x_{ini}, y) = f(y)$, and the boundary data on $y = y_o$, $u(x, y_o) = g(x)$. For analytical simplicity, we assume $k = k_o - j\epsilon$, $\epsilon > 0$. The lossless case which we are considering in the thesis can be considered as the limit of the lossy case as $\epsilon \to 0$. Using the Fourier sine integral, it is shown in [Ref. 2] that

$$\frac{\partial u}{\partial y}u(x,y)\Big|_{y=y_o} = \sqrt{\frac{2jk}{\pi}}\left[\frac{1}{\sqrt{x-x_{ini}}}\int_{\tau=y_o}^{\infty}f_\tau(\tau)e^{-jk(\tau-y_o)^2/2(x-x_{ini})}d\tau - \int_{\tau=x_{ini}}^{x-x_{ini}}\frac{g_\tau(\tau)}{\sqrt{x-\tau}}d\tau\right]. \tag{23}$$

The integrals can be evaluated approximately by replacing the derivatives with differences. Figure 3 shows data points on the line $y = y_o$ and on the portion of $x = x_{ini}$ which is above $y = y_o$.
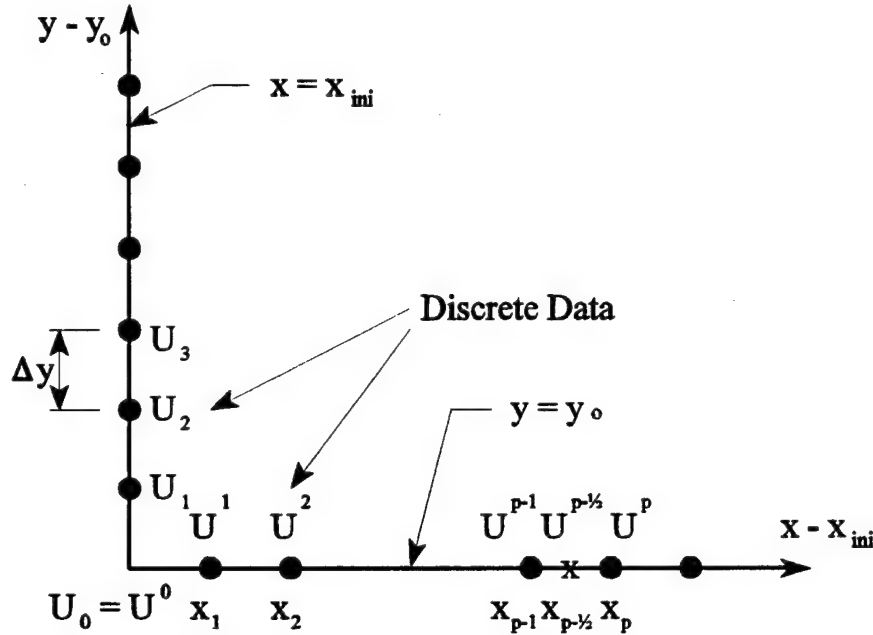
Figure 3.   Discrete derivatives for integral evaluations.

Consider the evaluation of $\partial u/\partial y|_{y=yo}$ at $x - x_{ini} = x_{p-\frac{1}{2}}$ with initial data on the line $x = x_{ini}$. Let us assume that this initial data is known on a uniform grid $y_m = y_o + m\Delta y$, $m = 0, 1, \cdots$. The derivative in the interval (y_{m-1}, y_m) can be approximated by the forward difference formula

$$\frac{\partial f(y)}{\partial y} \approx \frac{u_m - u_{m-1}}{\Delta y} \; ; \qquad y \in (y_{m-1}, y_m), \tag{24}$$

where $u_m = u(x_{ini}, y_m)$. Then

$$\frac{1}{\sqrt{x}}\int_{\tau=y_{m-1}}^{y_m} f_\tau(\tau)e^{-jk(\tau-y_o)^2/2(x-x_{ini})}d\tau \; = \; \sum_{m=1}^{\infty}\left(\frac{u_m - u_{m-1}}{\Delta y}\right)\sqrt{\frac{\pi}{k}}$$

$$\left[F\left(\sqrt{\frac{k}{\pi(x-x_{ini})}}(y_m-y_o)\right) - F\left(\sqrt{\frac{k}{\pi(x-x_{ini})}}(y_{m-1}-y_o)\right)\right] ,\tag{25}$$

where $F(x) = \int_0^x e^{-j(\pi/2)\tau^2} d\tau$ is a complex Fresnel integral [Ref. 6].

Now, consider the boundary data on the line $y = y_o$. Assume a non-uniform grid x_{ini}, $x_{ini} + x_1$, $x_{ini} + x_2 \cdots$, $x_{ini} + x_{p-\frac{1}{2}} = x$. On the interval $x - x_{ini} = (x_{m-1}, x_m)$, the derivative can be approximated as

$$g_\tau(\tau) = \frac{u^m - u^{m-1}}{x_m - x_{m-1}}, \tag{26}$$

where $u_m = u(x_m, y_o)$. The second integral in Eq. (23) can now be obtained as

$$\int_{\tau - x_{ini}}^{x_{ini} + x_{p-\frac{1}{2}}} \frac{g_\tau(\tau)}{\sqrt{x_{ini} + x_{p-\frac{1}{2}} - \tau}} d\tau = 2 \sum_{m-1}^{p-1} \frac{u^m - u^{m-1}}{\sqrt{x_{p-\frac{1}{2}} - x_{m-1}} + \sqrt{x_{p-\frac{1}{2}} - x_m}} + 2 \frac{u^{p-\frac{1}{2}} - u^{p-1}}{\sqrt{x_{p-\frac{1}{2}} - x_{p-1}}}. \tag{27}$$

Substituting Eq. (25) and (27) into Eq. (23),

$$\frac{\partial u}{\partial y}\bigg|_{y \to y_o}^{x \to x_{ini} + x_{p-\frac{1}{2}}} + \sqrt{\frac{8jk}{\pi(x_{p-\frac{1}{2}} - x_{p-1})}} \, u\bigg|_{y \to y_o}^{x \to x_{ini} + x_{p-\frac{1}{2}}}$$

$$= \frac{\sqrt{2j}}{\Delta y} \sum_{m-1}^{\cdot} (u_m - u_{m-1}) \left[F\left(\sqrt{\frac{k}{\pi(x_{p-\frac{1}{2}} - x_{ini})}} \, (y_m - y_o) \right) - F\left(\sqrt{\frac{k}{\pi(x_{p-\frac{1}{2}} - x_{ini})}} \, (y_{m-1} - y_o) \right) \right]$$

$$- \sqrt{\frac{8jk}{\pi}} \sum_{m-1}^{p-1} \frac{u^m - u^{m-1}}{\sqrt{x_{p-\frac{1}{2}} - x_m} + \sqrt{x_{p-\frac{1}{2}} - x_{m-1}}} + \sqrt{\frac{8jk}{\pi(x_{p-\frac{1}{2}} - x_{p-1})}} \cdot u^{p-1}, \tag{28}$$

where $x_{p-\frac{1}{2}} = \frac{1}{2}(x_{p-1} + x_p) \Rightarrow x_{p-\frac{1}{2}} - x_{p-1} = \frac{1}{2}(x_p - x_{p-1}) \triangleq \frac{1}{2}\Delta x_{p-1}$. Equation (28) can be thought of as the discrete version of a continuous boundary condition of the form

$$\frac{\partial u}{\partial y} + r(x)u = s(x), \tag{29}$$

where

12

$$r(x) = \sqrt{\frac{8jk}{\pi}} \, \frac{1}{\sqrt{x - x_{p-1}}} \,, \tag{30}$$

$$s(x) = \sqrt{2j} \sum_{m-1}^{\infty} \frac{u_m - u_{m-1}}{\Delta y} \left[F\left(\sqrt{\frac{k}{\pi(x - x_{ini})}}(y_m - y_o)\right) - F\left(\sqrt{\frac{k}{\pi(x - x_{ini})}}(y_{m-1} - y_o)\right) \right]$$

$$- \sqrt{\frac{8jk}{\pi}} \sum_{m-1}^{p-1} \frac{u^m - u^{m-1}}{\sqrt{x - x_m} + \sqrt{x - x_{m-1}}} + \sqrt{\frac{8jk}{\pi(x - x_{p-1})}} \cdot u^{p-1} \,. \tag{31}$$

D. TRANSFORMATION TO A CURVILINEAR COORDINATE SYSTEM

The partial differential equation in Eq. (17) and the boundary conditions in Eqs. (21) and (28) will now be transformed to a curvilinear coordinate system. Consider the narrow angle parabolic PDE given by Eq. (17)

$$u_x = \frac{1}{2jk_o} \frac{\partial^2 u}{\partial y^2} \,, \tag{32}$$

together with the tropospheric boundary condition

$$\frac{\partial}{\partial y} u(x_m, y_0) + r(x_m) u(x_m, y_0) = s(x_m, y_0), \tag{33}$$

and the impedance boundary condition on the irregular boundary

$$u_v + c_1 u = 0. \tag{34}$$

We will cast all of these equations in a curvilinear coordinate system (ξ, η) shown in Fig. 4. This will permit accurate imposition of boundary conditions. Note that the parabolic nature of the equation will not change as a result of the transformation. The irregular terrain boundary will map into $\eta = 0$ and the upper boundary into $\eta = N$ (integer). The entire coordinate system is generated by the specification of the terrain geometry.

Assuming the transformation $x = x(\xi)$, $y = y(\xi, \eta)$, and using the various metrics needed [Ref. 7], Eq. (32) becomes

$$u_\xi = \left[\left(- \frac{y_{\eta\eta}}{y_\eta^3} \right) \frac{x_\xi}{2jk_o} + \frac{y_\xi}{y_\eta} \right] u_\eta + \frac{x_\xi}{2jk_o y_\eta^2} u_{\eta\eta} . \tag{35}$$
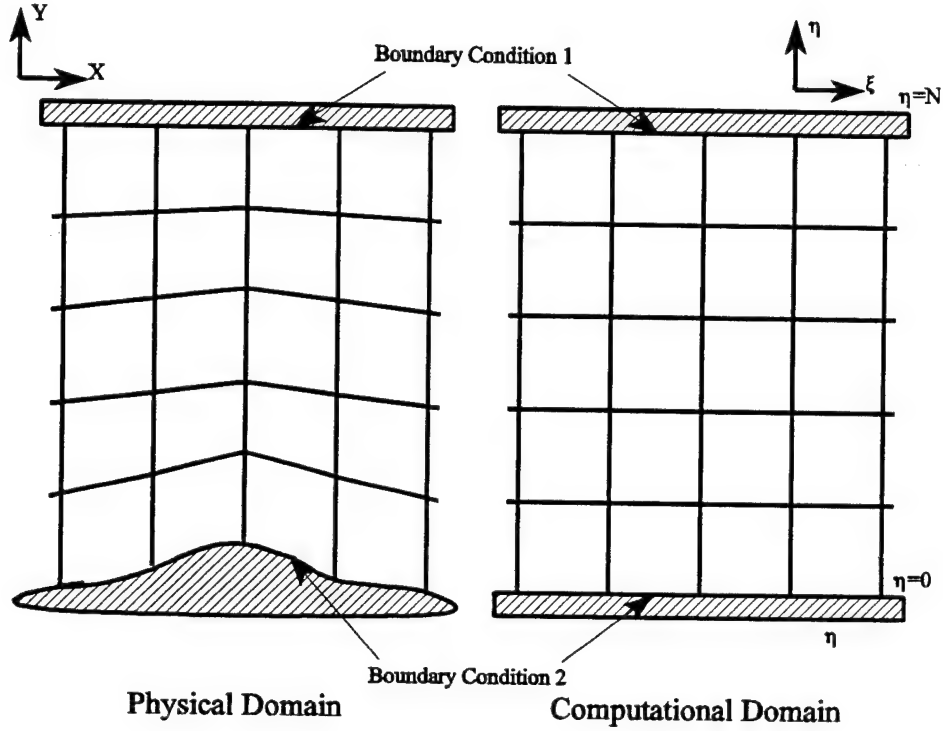
Figure 4. Curvilinear coordinate system.

Letting

$$b_2 = \frac{x_\xi}{y_\eta} \left[\left(- \frac{y_{\eta\eta}}{y_\eta^2} \right) \frac{1}{2jk_o} + \frac{y_\xi}{x_\xi} \right] , \tag{36}$$

$$b_3 = \frac{x_\xi}{2jk_o y_\eta^2} , \tag{37}$$

then Eq. (35) can be expressed as

$$u_\xi = b_2 u_\eta + b_3 u_{\eta\eta} . \tag{38}$$

The normal derivative on a η = constant line is

14

$$u_v(\eta = \text{constant}) = \frac{\sqrt{x_\xi^2 + y_\xi^2}}{x_\xi y_\eta - y_\xi x_\eta} u_\eta - \frac{x_\xi x_\eta + y_\xi y_\eta}{\sqrt{x_\xi^2 + y_\xi^2} (x_\xi y_\eta - y_\xi x_\eta)} u_\xi .$$ (39)

Using

$$\cos\theta = \frac{x_\xi}{\sqrt{x_\xi^2 + y_\xi^2}} \quad \text{and} \quad \sin\theta = \frac{y_\xi}{\sqrt{x_\xi^2 + y_\xi^2}} ,$$ (40)

the boundary condition at the bottom boundary $u_v + c_l u = 0$ gets transformed for $x_\eta = 0$ to

$$u_v - \frac{y_\eta}{x_\xi}\sin\theta\cos\theta u_\xi + c_l y_\eta \cos\theta u = 0.$$ (41)

Similarly, the boundary condition at $y = y_o$ gets transformed to

$$u_\eta(\xi_m, N) + r(\xi_m, N)y_\eta(\xi_m)u(\xi_m, N) = y_\eta s(\xi_m, N).$$ (42)

III. SOLUTION PROCEDURE

In the previous chapter we presented the underlying equations and the relevant boundary conditions for the computation of fields over an irregular terrain. In Section A of this chapter, we present details on the generation of the coordinate system. In Section B, we adopt the Crank-Nicolson scheme in the transformed domain to obtain the required finite difference equations.

A.   GENERATION OF THE CURVILINEAR COORDINATE SYSTEM

Consider the computational domain between the terrain profile and a horizontal upper boundary. We treat the terrain profile as being comprised of piece-wise linear functions and consider a horizontal upper boundary as shown in Fig. 5. We wish to generate a coordinate system (ξ, η) such that the lower and the upper boundaries correspond to constant η lines. The coordinate lines gradually become horizontal as one proceeds from the lower to the upper boundary. Specification of the lower and upper boundaries completely determines our coordinate system. Without loss of generality, we will choose the increments between the mesh points in the (ξ, η) plane to be unity. Figure 5(a) shows the mesh points in the physical domain and Fig. 5(b) in the computational domain. Figure 6 shows corresponding pairs of points on the upper and lower boundaries in the physical and computational domains. The (x, y) coordinates of an interior point are generated by using linear interpolation. Letting $\Delta x_i = (x_{i+1} - x_i)$, $\Delta y_i = (y_{i+1} - y_i)$, and $\Delta \xi_i = (\xi_{i+1} - \xi_i)$, the parametric equations for x and y are [Ref. 2]

$$x(\xi) = x_i + \frac{\Delta x_i}{\Delta \xi_i}(\xi - \xi_i), \tag{43}$$

$$y(\xi, \eta) = \left(1 - \frac{\eta}{N}\right)\left[y_i + \frac{\Delta y_i}{\Delta \xi_i}(\xi - \xi_i)\right] + \frac{\eta}{N}y_o, \tag{44}$$

for $\xi_i \leq \xi \leq \xi_{i+1}$, $0 \leq \eta \leq N$.

17
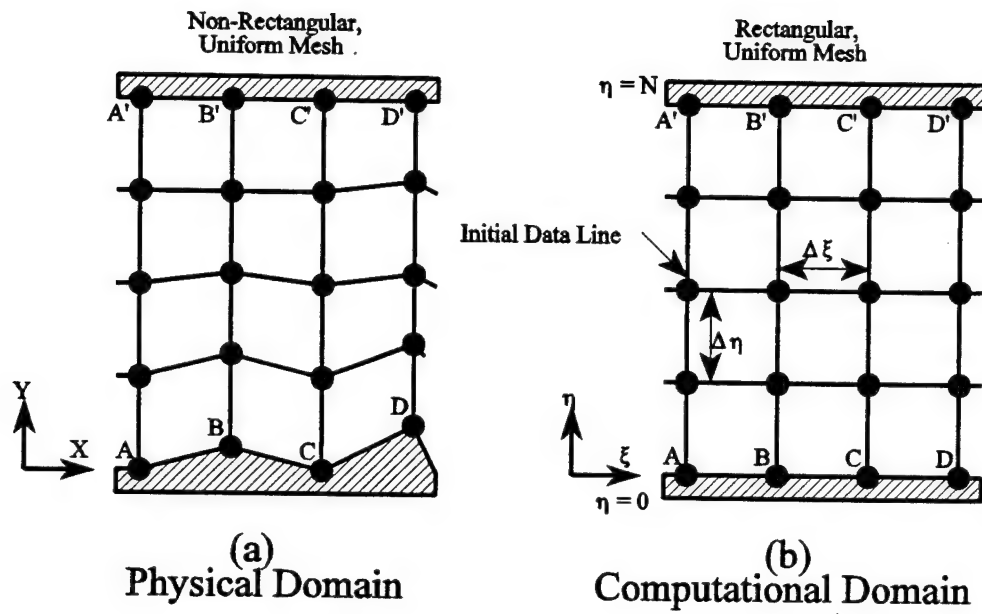
Figure 5.   Physical and computational grids.
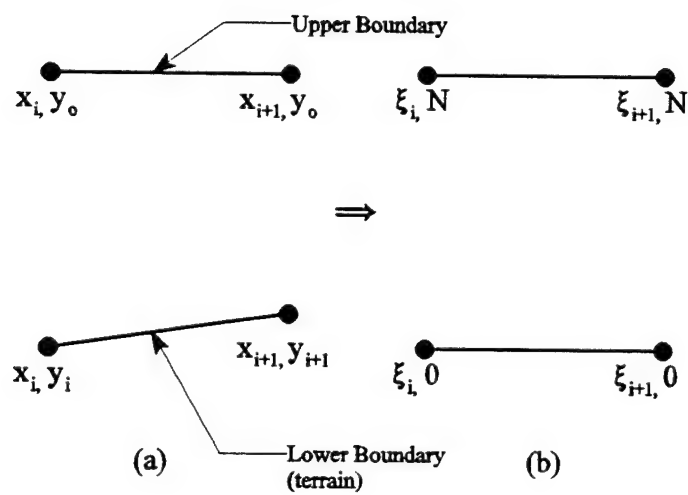
Figure 6.   Physical and computational domain segments.

It is possible to generalize this to any ground profile shape of the form $f(x)$ by writing

$$y = \left(1 - \frac{\eta}{N}\right) f(x) + \frac{\eta}{N} y_o = \left(1 - \frac{\eta}{N}\right) f[x(\xi)] + \frac{\eta}{N} y_o, \tag{45}$$

with $x(\xi)$ given as above. However, we choose the piece-wise linear form for its ability to model discrete sets of data on the ground. At any interior point, $\xi_i < \xi < \xi_{i+1}$, the various metrics are obtained as

$$x_\xi = \frac{\Delta x_i}{\Delta \xi_i}, \qquad x_\eta = 0, \tag{46}$$

$$y_\xi = \left(1 - \frac{\eta}{N}\right) \frac{\Delta y_i}{\Delta \xi_i}, \qquad y_\eta = \frac{1}{N}\left[y_o - y_i - \frac{\Delta y_i}{\Delta \xi_i}(\xi - \xi_i)\right], \qquad y_{\eta\eta} = 0. \tag{47}$$

At the junction points $\xi = \xi_i$ or ξ_{i+1}, we use the central difference formulas

$$x_\xi(\xi = \xi_{i+1}) = \frac{x_{i+2} - x_i}{\xi_{i+2} - \xi_i} = \frac{\Delta x_{i+1} + \Delta x_i}{\Delta \xi_{i+1} + \Delta \xi_i}, \tag{48}$$

$$y_\xi(\xi = \xi_{i+1}) = \left(1 - \frac{\eta}{N}\right) \frac{\Delta y_{i+1} + \Delta y_i}{\Delta \xi_{i+1} + \Delta \xi_i}. \tag{49}$$

Note that the analytical expression yields a discontinuous value for these derivatives. We use the analytical expressions only to generate grid points and use the central difference formulas to arrive at the derivatives with respect to ξ. In other words, once the grid points are generated on the lines AA', BB', ... , etc., we assume that the space is smoothly connected through the grid points. In the numerical implementation using the Crank-Nicolson implicit scheme [Ref. 8], the metrics are needed at the midpoint with respect to ξ, i.e., at $\xi = \xi_i + \Delta \xi_i/2$, and the interior point formulas are applicable. For a uniform mesh in the computational domain, $\Delta \xi_i = 1$, $\eta = q$, $q = 0, 1, 2, ... , N$.

19

$$x_\xi = \Delta x_P \tag{50}$$

$$y_\xi = \left(1 - \frac{q}{N}\right)\Delta y_P \tag{51}$$

$$y_\eta = \frac{1}{N}\left(y_o - \frac{y_{i+1} + y_i}{2}\right), \tag{52}$$

$$y = \left(1 - \frac{q}{N}\right)\left(\frac{y_{i+1} + y_i}{2}\right) + \frac{q}{N}y_o. \tag{53}$$

Figure 7 shows an example of the curvilinear mesh for a Gaussian shaped ridge on flat ground. Note that the vertical increment is constant on any vertical line, but varies from line to line.
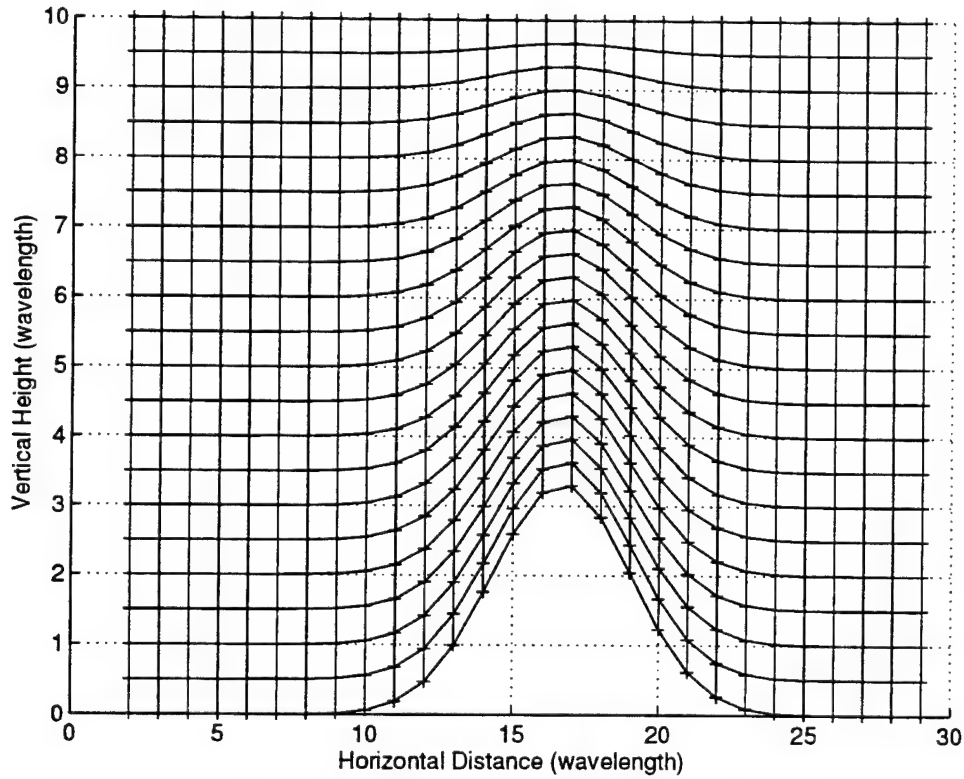
Figure 7. Curvilinear mesh for a Gaussian shaped ridge on flat ground.

20

B. NUMERICAL IMPLEMENTATION USING THE CRANK-NICOLSON SCHEME

Consider the narrow angle parabolic PDE together with the boundary conditions given by Eqs. (38), (41), and (42). We would like to implement the equations using a Crank-Nicolson implicit scheme [Ref. 8]. We will write different forms for the internal and boundary regions. The grid points for an internal region in the computational domain are shown in Fig. 8. Given the field data on the line p-1, we would like to predict the field on the line p.
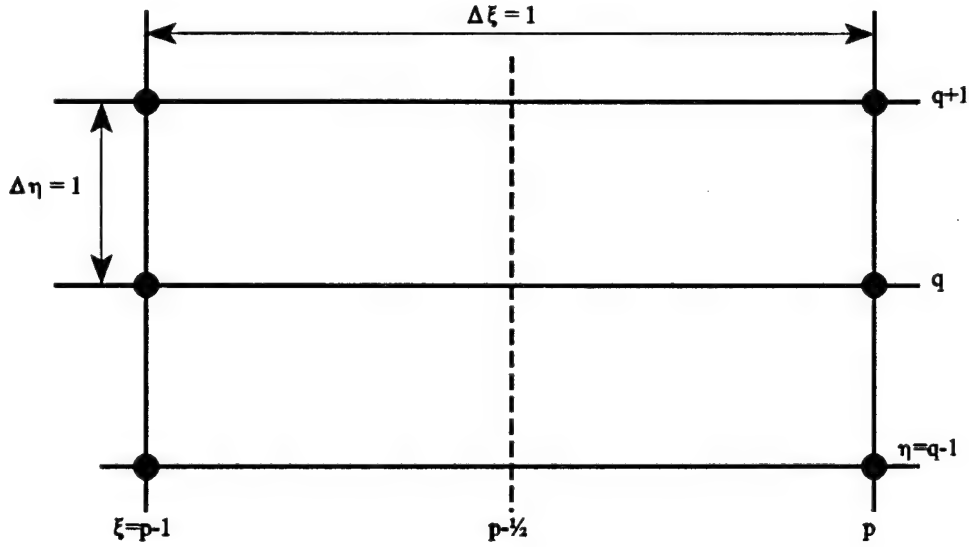
Figure 8.   Internal grid points in computational domain.

Using the notation $u_q^p = u(p,q) = u(x_p, y_q)$, the various derivatives (assuming $\Delta \xi = \Delta \eta = 1$) are

$$u_\xi(p-\tfrac{1}{2}, q) = u_q^p - u_q^{p-1}, \tag{54}$$

$$u_\eta(p-\tfrac{1}{2},q) = \tfrac{1}{4}[u_{q+1}^{p-1} + u_{q+1}^{p} - (u_{q-1}^{p-1} + u_{q-1}^{p})], \qquad (55)$$

$$u_{\eta\eta}(p-\tfrac{1}{2},q) = \tfrac{1}{2}[u_{q+1}^{p} - 2u_{q}^{p} + u_{q+1}^{p} + u_{q-1}^{p-1} - 2u_{q}^{p-1} + u_{q-1}^{p-1}]. \qquad (56)$$

Substituting into Eq. (43) and rearranging the terms, we get [Ref. 2]

$$\frac{1}{2}\left(\frac{b_2}{2} + b_3\right)u_{q+1}^{p} - \left(1 + b_3\right)u_{q}^{p} + \frac{1}{2}\left(b_3 - \frac{b_2}{2}\right)u_{q-1}^{p}$$

$$+ \frac{1}{2}\left(\frac{b_2}{2} + b_3\right)u_{q+1}^{p-1} + \left(1 - b_3\right)u_{q}^{p-1} + \frac{1}{2}\left(b_3 - \frac{b_2}{2}\right)u_{q-1}^{p-1} = 0. \qquad (57)$$

Letting

$$\alpha = \tfrac{1}{2}(b_3 + \tfrac{1}{2}b_2)_q^{p-\frac{1}{2}}, \qquad (58)$$

$$\beta = (b_3)_q^{p-\frac{1}{2}}, \qquad (59)$$

$$\gamma = \tfrac{1}{2}(b_3 - \tfrac{1}{2}b_2)_q^{p-\frac{1}{2}}, \qquad (60)$$

we have for $p = 1, 2, \cdots; q = 1, 2, \cdots, N-1$

$$\alpha u_{q+1}^{p} - (1 + \beta)u_{q}^{p} + \gamma u_{q-1}^{p} = -\alpha u_{q+1}^{p-1} - (1 - \beta)u_{q}^{p-1} - \gamma u_{q-1}^{p-1}. \qquad (61)$$

We will extend the applicability of this equation to include $q = 0$ and $q = N$ to accommodate the derivative boundary conditions on the lower and upper boundaries. For $q = 0$, we have

$$\alpha u_{1}^{p} - (1 + \beta)u_{0}^{p} + \gamma u_{-1}^{p} = -\alpha u_{1}^{p-1} - (1 - \beta)u_{0}^{p-1} - \gamma u_{-1}^{p-1}. \qquad (62)$$

For $q = N$, we have

$$\alpha u_{N+1}^{p} - (1 + \beta)u_{N}^{p} + \gamma u_{N-1}^{p} = -\alpha u_{N+1}^{p-1} - (1 - \beta)u_{N}^{p-1} - \gamma u_{N-1}^{p-1} \qquad (63)$$

22
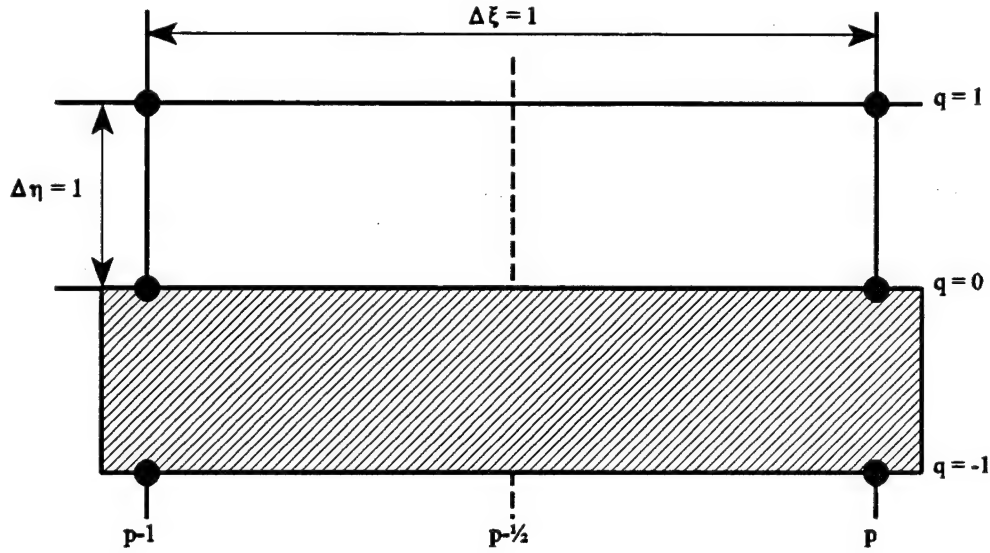
Figure 9.   Grid points at the lower boundary.

Figure 9 shows the grid points at the lower boundary. We use central differences for the boundary condition in Eq. (41) and combine with Eq. (62) to get

$$\alpha' u_1^P - (1 + \beta') u_0^P = -\alpha' u_1^{P-1} - (1 - \beta'') u_0^{P-1}, \tag{64}$$

where

$$\alpha' = \alpha + \gamma, \tag{65}$$

$$\beta' = \beta - 2\gamma y_\eta \cos \theta \left(c_1 - \frac{2\sin \theta}{x_\xi} \right), \tag{66}$$

$$\beta'' = \beta - 2\gamma y_\eta \cos \theta \left(c_1 + \frac{2\sin \theta}{x_\xi} \right). \tag{67}$$

We have also tried to use one-sided forward difference formulas near the terrain, but the results were less accurate than with the central difference scheme. Results for the two approaches will be compared in the next chapter.

23
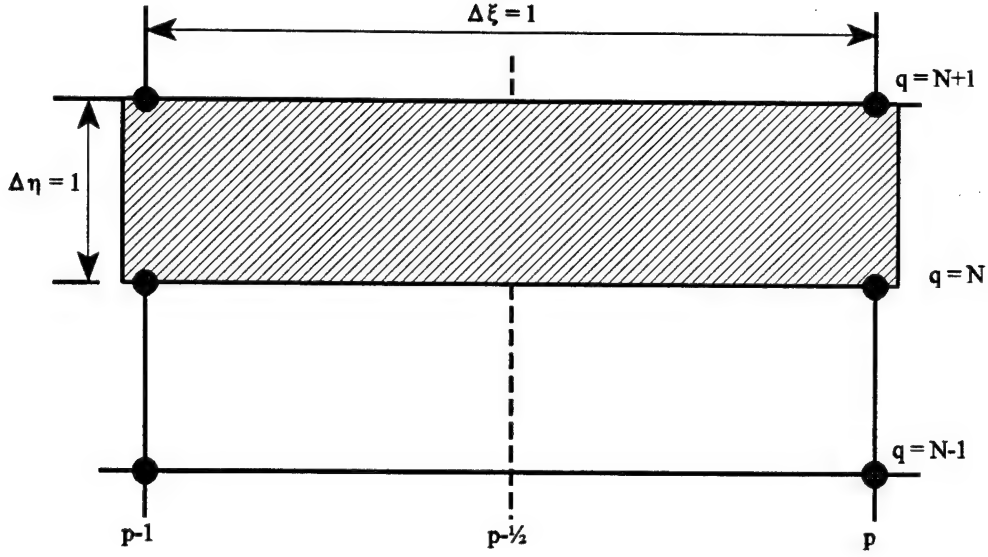
Figure 10.   Grid points at the upper boundary.

Similarly, using central differences for the tropospheric boundary condition in Eq. (42) and combining with Eq. (63) results in

$$(1 + \lambda)u_N^p - \gamma'u_{N-1}^p = (1 - \lambda)u_N^{p-1} + \gamma'u_{N-1}^{p-1} + 4\alpha y_\eta s^{p-\frac{1}{2}}. \tag{68}$$

where

$$\lambda = \beta + y_\eta 8\alpha \sqrt{\frac{jk}{\pi \Delta x_{p-1}}} \ ,$$

$$\gamma' = \gamma + \alpha,$$

$$\Delta x_{p-1} = x_p - x_{p-1}, \qquad x_{p-\frac{1}{2}} = x_{p-1} + \frac{1}{2}\Delta x_{p-1} = \frac{1}{2}(x_p + x_{p-1}),$$

24

$$s^{p-\frac{1}{2}} = \frac{\sqrt{2j}}{\Delta y} \overset{-}{\sum_{m-1}} (u_m - u_{m-1}) \left[F\left(\sqrt{\frac{k}{\pi x_{p-\frac{1}{2}}}} y_m\right) - F\left(\sqrt{\frac{k}{\pi x_{p-\frac{1}{2}}}} y_{m-1}\right) \right]$$

$$- \sqrt{\frac{8jk}{\pi}} \sum_{m-1}^{p-1} \frac{u_N^m - u_N^{m-1}}{(\sqrt{x_{p-\frac{1}{2}} - x_m} + \sqrt{x_{p-\frac{1}{2}} - x_{m-1}})} + \sqrt{\frac{16jk}{\pi \Delta x_{p-1}}} u_N^{p-1}.$$

We augment Eq. (61) for $q = 1, 2, \cdots, N\text{-}1$ with Eq. (64) and (68) for $q = 0$ and $q = N$ respectively to define the equations for $q = 0, 1, 2, \cdots, N$. The system of equations so defined can be expressed as a matrix equation of the form

$$
\begin{bmatrix}
X & X & & & & \\
X & X & X & & & \\
& X & X & X & & \\
& & & \vdots & & \\
& & & \vdots & & \\
& & & & X & X
\end{bmatrix}
\begin{bmatrix}
u_0^p \\
u_1^p \\
\vdots \\
\vdots \\
\vdots \\
u_N^p
\end{bmatrix}
=
\begin{bmatrix}
X & X & & & & \\
X & X & X & & & \\
& X & X & X & & \\
& & & \vdots & & \\
& & & & X & X
\end{bmatrix}
\begin{bmatrix}
u_0^{p-1} \\
u_1^{p-1} \\
\vdots \\
\vdots \\
u_N^{p-1}
\end{bmatrix}
+
\begin{bmatrix}
0 \\
\ddots \\
\ddots \\
\ddots \\
4\alpha y_\eta s^{p-\frac{1}{2}}
\end{bmatrix} \quad (69)
$$

where X denotes a non-zero entry. The tri-diagonal matrix on the left hand side of Eq. (69) can be inverted efficiently to yield a solution on line $\xi = \xi_p$ in terms of the field values on the line $\xi = \xi_{p-1}$. Equation (69) can be used to march forward in range starting from initial data specified at $\xi = 0$ ($x = x_{ini}$).

IV. COMPARISON OF RESULTS

Having presented the basic theory in the previous chapters, we will present numerical results in this chapter. The overall accuracy of the solution depends on a number of parameters such as the step size, location of the tropospheric boundary (i.e., y_0 in Fig. 1), the region above the tropospheric boundary, and the differencing scheme used at the boundaries. In this chapter we will make a systematic study on the dependence of the solution on various parameters. Section A.1 compares the results of the forward versus central differencing schemes for implementing the lower boundary condition. Sections A.2 and A.3 show the effects of horizontal and vertical step sizes, respectively. In Section A.4, we present the effect of the placement of the tropospheric boundary condition. In the remaining sections, we present comparisons with the results available in the literature for specific obstacles.

A.   PARAMETRIC STUDY OF THE FINITE DIFFERENCE SCHEME

1.   Forward-Difference versus Central Difference Scheme for the Impedance Boundary Condition

In the implementation using the Crank-Nicolson implicit scheme, the derivatives at any interior point are approximated using the central difference formulas. This approximation is also extended to the lower boundary given in Eq. (69). Alternatively, the derivatives at the lower boundary could also be approximated using the forward difference formulas. From Eq. (43) and using the forward difference formulas, we have

$$\frac{1}{2}[(u_1^P - u_0^P) + (u_1^{P-1} - u_0^{P-1})] - \left(\frac{y_\eta}{x_\xi}\cos\theta\sin\theta\right)(u_0^P - u_0^{P-1})$$

$$+ (c_1 y_\eta \cos\theta)\left(\frac{u_0^P + u_0^{P-1}}{2}\right) = 0. \tag{70}$$

Equation (70) can be written as

$$\alpha' u_1^P - (1 + \beta')u_0^P = -\alpha' u_1^{P-1} + (1 - \beta'')u_0^{P-1}, \tag{71}$$

27

where

$$\alpha' = 1, \qquad \beta' = y_\eta \cos\theta \left(\frac{2\sin\theta}{x_\xi} - c_1 \right), \qquad \beta'' = y_\eta \cos\theta \left(\frac{2\sin\theta}{x_\xi} + c_1 \right) . \qquad (72)$$

Numerical results using both the central difference and forward difference schemes were used to compute magnetic field due to a vertically polarized line source on the surface of a PEC plane. The results of both schemes are compared with the exact solution [Ref. 9] and plotted in Fig. 11 (magnitude of magnetic field, Hz, on the surface of the PEC plane), Fig. 12 (Hz @ Height = 0.1λ), and Fig. 13 (Hz @ Height = $y_o = 20\lambda$). It is observed that the central difference scheme produces a solution that agrees better with the exact solution. The solution using forward differences exhibits spurious oscillations which could not be resolved. Henceforth we will adopt the central difference scheme for the subsequent test cases shown.

2. Variation in Horizontal Step Size (With Fixed Vertical Step Size)

The Crank-Nicolson scheme has the advantage of being valid (i.e., convergent and stable) for all finite values of the horizontal step size for a cartesian mesh. To verify the validity of the scheme with respect to horizontal step sizes, numerical results were evaluated for three different horizontal step sizes ($\Delta x = 0.1\lambda$, $\Delta x = 0.2\lambda$, and $\Delta x = 0.5\lambda$) with a fixed vertical step size of $\Delta y = 0.1\lambda$. The magnitude of the magnetic field, Hz, due to a vertically polarized line source placed at ($x0 = 0$, $y0 = 0$) on the surface of a PEC plane are computed numerically and plotted in Fig. 14 (Hz on the surface of the PEC plane) and Fig. 15 (Hz @ Height = $y_o = 20\lambda$). The plots show that the results are convergent for all the three horizontal step sizes, and excellent agreement is observed between the numerical results and the exact solution for the surface magnetic field. Minor oscillations are observed for magnitude of the magnetic field at the upper boundary. However, the average value of the magnetic field, Hz, is still close to the exact solution given by [Ref. 9]

$$H_z(x,y) = 2 \left[\frac{jk_o}{4} \frac{(\tilde{x} - \tilde{x}_o)}{\tilde{R}_o} H_1^{(2)}(\tilde{R}_o) \right] , \qquad (73)$$

where $\tilde{x} = k_o x$, $\tilde{x}_o = k_o x_o$, $\tilde{R}_o = k_o\sqrt{(x - x_o)^2 + (y - y_o)^2}$, and $H_l^{(2)}$ is the Hankel function of the second kind of order 1.

3. Variation in Vertical Step Size (With Fixed Horizontal Step Size)

Next, we investigate the behavior of the Crank-Nicolson scheme with respect to vertical step size. In this study, the numerical results were evaluated for three different vertical step sizes ($\Delta y = 0.1\lambda$, $\Delta y = 0.2\lambda$, and $\Delta y = 0.5\lambda$) with a fixed horizontal step size of $\Delta x = 0.1\lambda$. The same profile of a vertically polarized line source placed at ($x0 = 0$, $y0 = 0$) on the surface of a PEC plane is adopted, and the magnitude of the magnetic field, Hz, are computed numerically. The results are plotted in Fig. 16 (Hz on the surface of the PEC plane) and Fig. 17 (Hz @ Height = y_o = 20λ). Again the plots show that the results at the surface are convergent for all the three vertical step sizes tested, and excellent agreement is observed between the numerical results and the exact solution for the magnetic field, Hz.

Minor oscillations are still observed at the upper boundary. Poor results are obtained with $\Delta y = 0.5\lambda$. This is possibly due to the inaccuracies of the upper boundary condition. Nonetheless, the numerical computation using step size of $\Delta x = \Delta y = 0.1\lambda$ produces results which are in good agreement with the exact solution.

4. Variation in the Tropospheric Boundary Condition Parameter

In the evaluation of $\partial u/\partial y|_{y=yo}$ at $x = x_{p-\frac{1}{2}}+x_{ini}$, we have considered and assumed that initial data is known on a uniform grid $y_m - y_o = m\Delta y$, $m = 0, 1, \cdots$. In practice we stop at some height $y_{ubc} > y_o$. To ascertain how high a point should be considered, we examine the cases of extending beyond the tropospheric boundary by 5λ, 10λ, and 20λ, (i.e., $y_{ubc} = y_o + 5\lambda$, 10λ, and 20λ). The simple test profile of the propagation of the magnetic field, Hz, due to a vertically polarized line source placed at ($x0 = 0$, $y0 = 0$) on the surface of a PEC plane are computed numerically. In this study we choose $\Delta x = \Delta y = 0.1\lambda$ and the upper boundary, y_o = 20λ. The results are plotted in Fig. 18 (Hz on the surface of the PEC plane) and Fig. 19 (Hz @ Height = y_o = 20λ). The plots show that the results are almost identical for all the three cases. To get an accurate representation of the tropospheric boundary condition, we need only to consider data on a vertical line which is within 5λ from the upper boundary. As such, all subsequent test cases will be computed using a tropospheric boundary with $y_{ubc} = y_o+5\lambda$.

29

Figure 11.   Surface magnetic field versus distance.

30
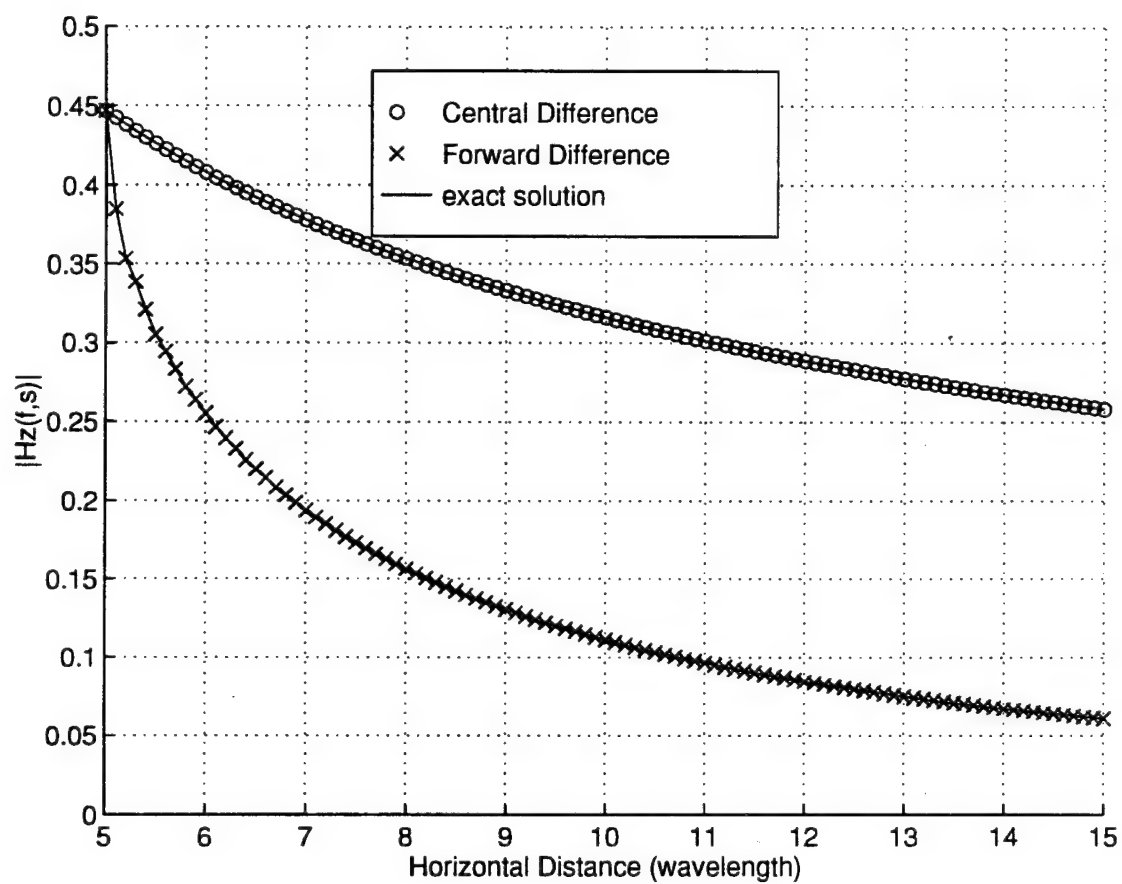
Figure 12. *Hz* versus distance @ height = 0.1λ.
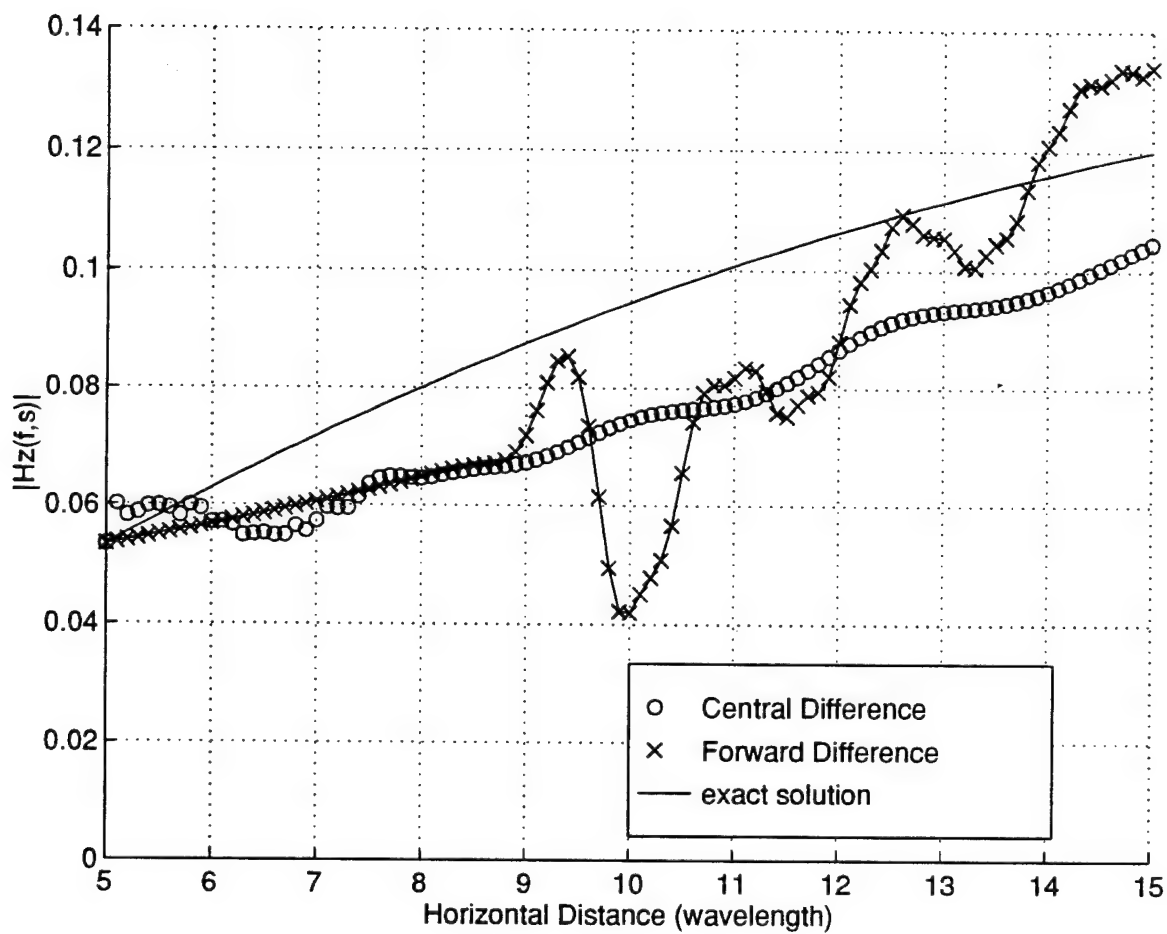
Figure 13. *Hz* versus distance @ height = $y_o = 20\lambda$.
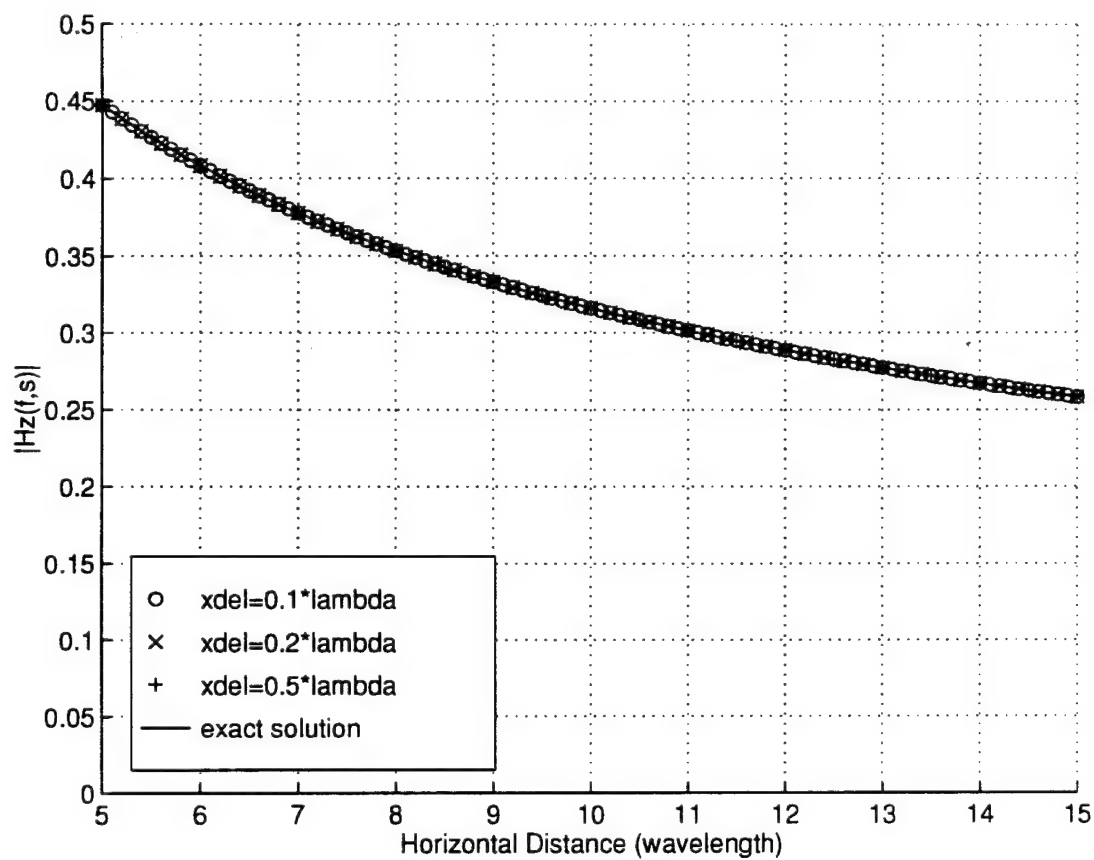
Figure 14.   Surface magnetic field versus distance.

33
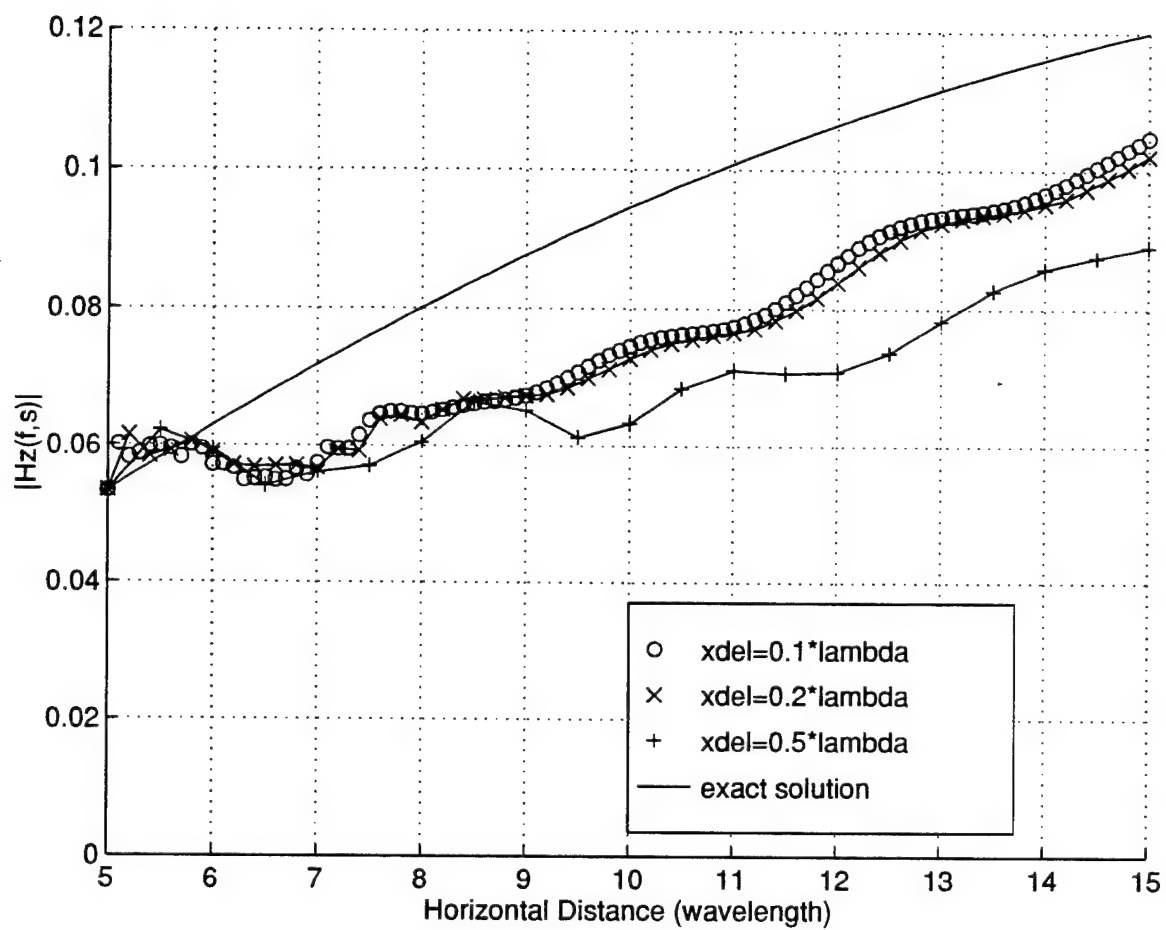
Figure 15.   *Hz* versus distance @ height = y_o = 20λ.

34
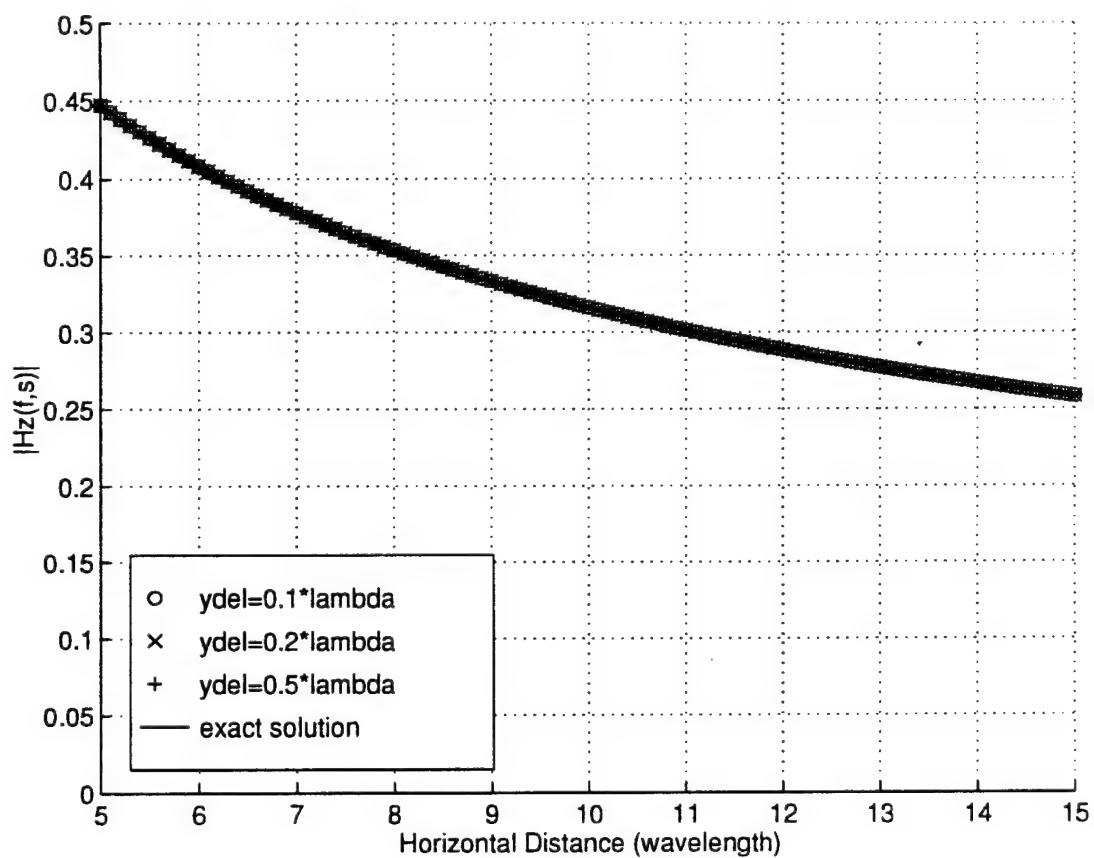
Figure 16. Surface magnetic field versus distance.
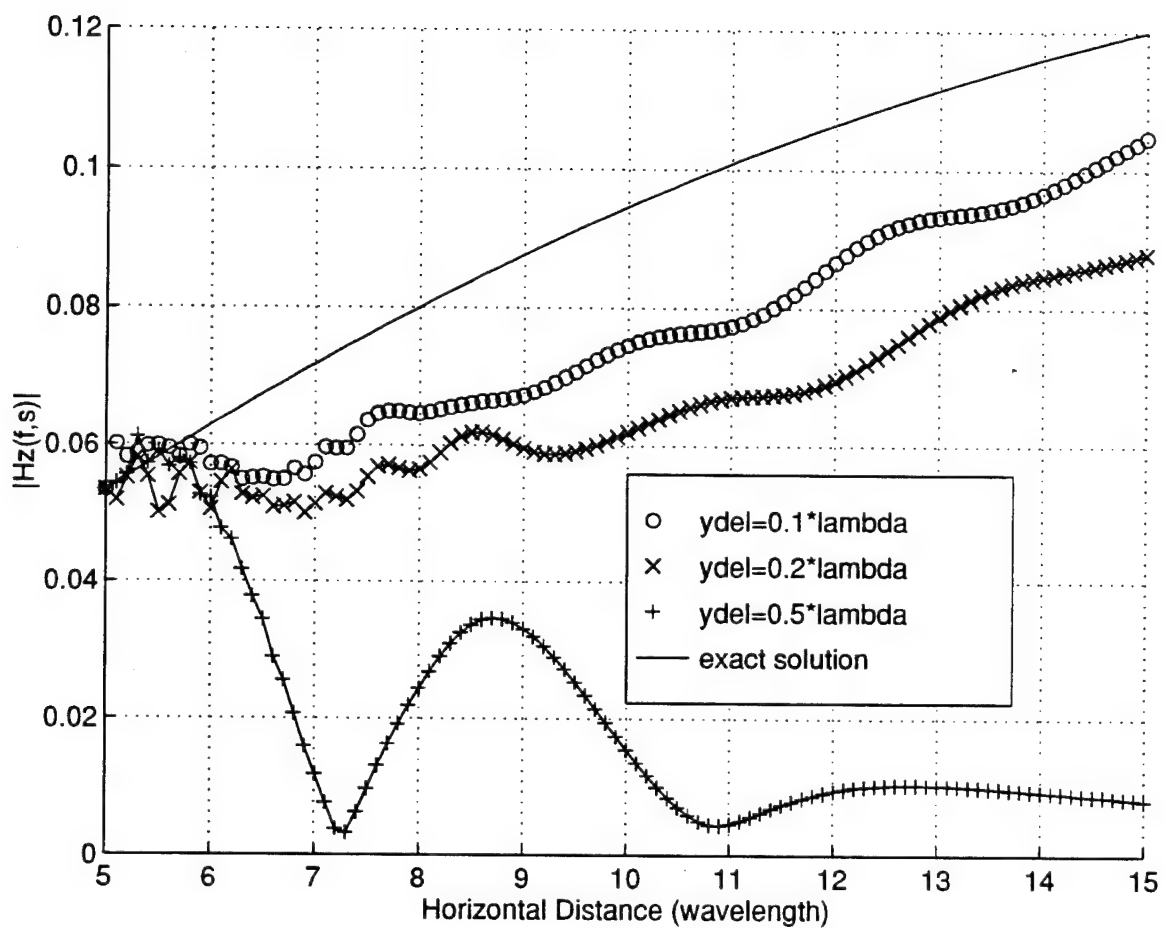
Figure 17. *Hz* versus distance @ height = y_o = 20λ.
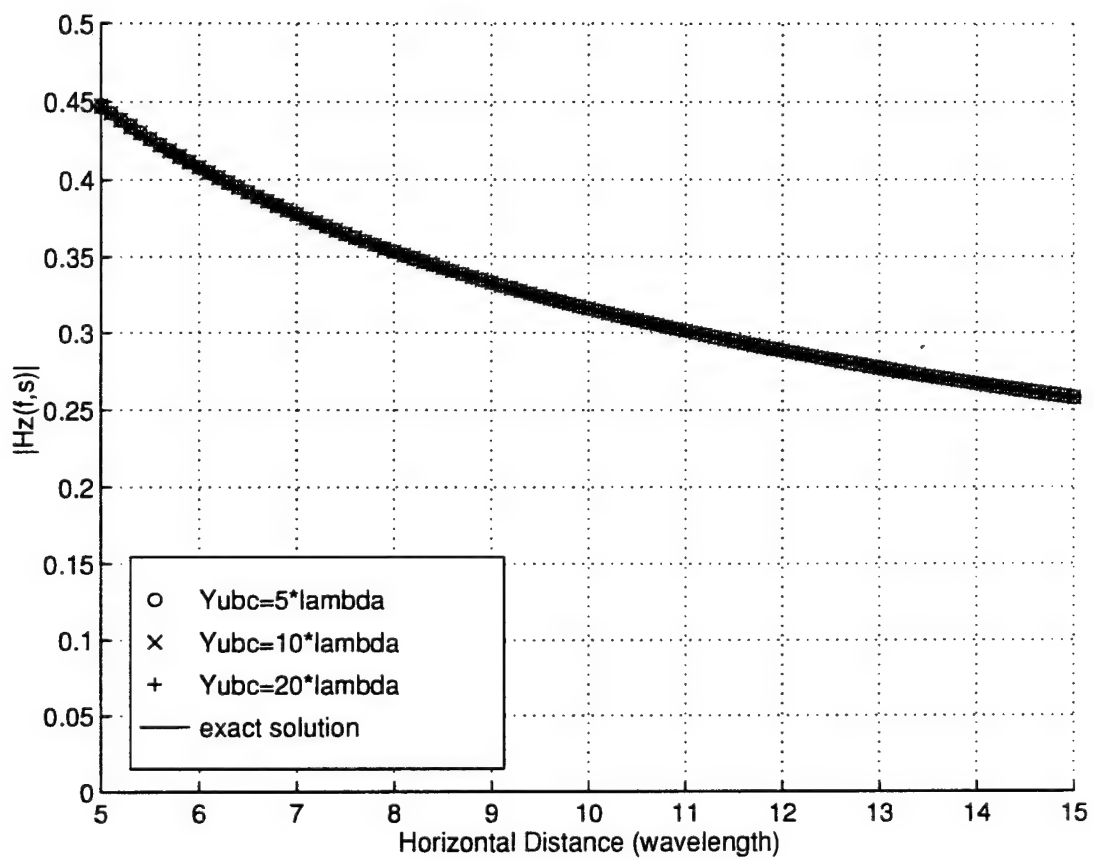
Figure 18. Surface magnetic field versus distance.
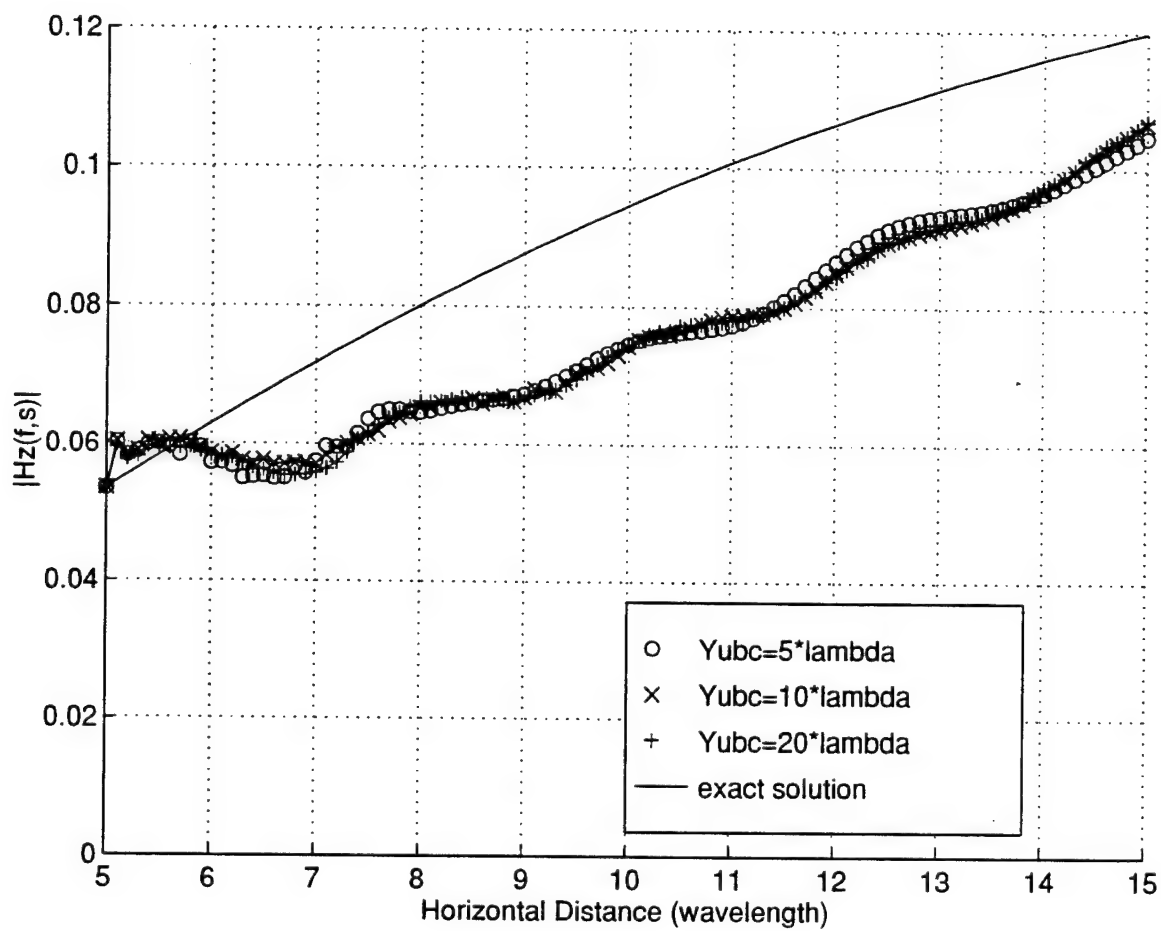
Figure 19. *Hz* versus distance @ height = $y_o = 20\lambda$.

38

B.   PROPAGATION OVER A PEC PLANE

In this section, we examine the effect of the height of the upper boundary, y_o, on the stability and accuracy of the numerical results. The magnitude of the magnetic field, Hz, due to a vertically polarized line source placed at $(x0 = 0, y0 = 0)$ on the surface of a PEC plane are computed numerically. In this study we choose $\Delta x = \Delta y = 0.1\lambda$ and $y_{ubc} = y_o + 5\lambda$. Results are presented for $y_o = 5\lambda$, 10λ, 20λ, and 30λ. The initial data line is at $x_{ini} = 5\lambda$, and the magnetic field is marched over a horizontal distance of 10λ.

1.   Magnetic Field Variation with Horizontal Distance

The variation in the magnitude of the magnetic field, Hz, along the horizontal distance on the surface of the PEC plane and at a height of 5λ is plotted in Fig. 20 and Fig. 21 respectively. We noticed that the oscillations are predominant when y_o is less than 20λ. For $y_o > 20\lambda$, the results are in good agreement with the exact solution.

2.   Magnetic Field Variation with Vertical Distance

Figures 22, 23, and 24 depict the results of the variations of the magnitude of the magnetic field, Hz, with vertical height at horizontal distances of 6λ, 10λ, and 15λ from the transmitter. Again, oscillations are present when the height of the upper boundary is below 20λ. More importantly, we observed that for a given horizontal distance, the deviations of the numerical results from the exact solution become more pronounced at higher points. This phenomenon is expected because the parabolic equation used in this thesis is valid for propagation angles close to horizontal $(\pm 15°)$. In fact the numerical result is fairly consistent with this restriction. For example, at a horizontal distance of 15λ from the transmitter (i.e., 10λ from the initial data line), the maximum height for which good results are expected is between 0 and 1.763λ. From Fig. 24, we see that this is true, and deviation between the numerical results and the exact solution begins at approximately 1.7λ. The same trend is also observed in Fig. 22 and 23. However, the difference between the numerical results and the exact solution increases with distance from the transmitter. This could be due to inaccuracies of the tropospheric boundary condition. The error in the tropospheric boundary condition is accumulative, and we would expect to see higher error at larger distances.

39
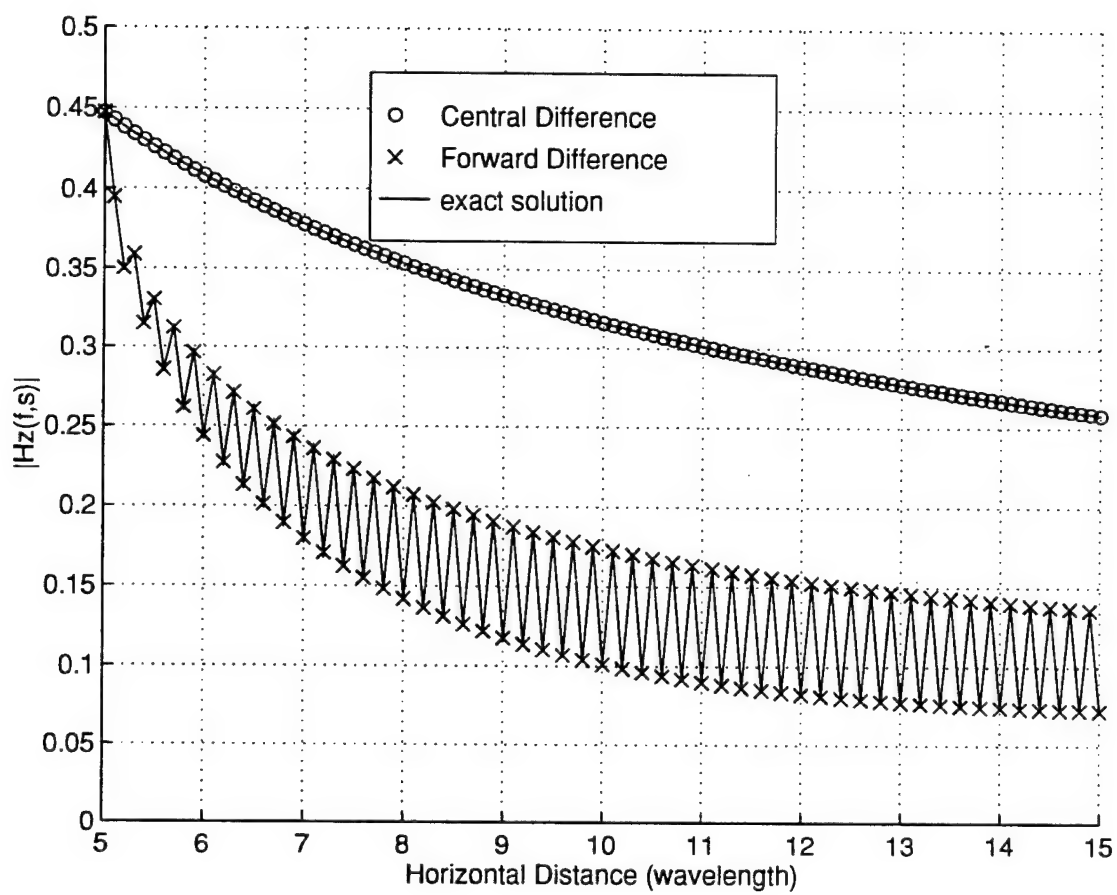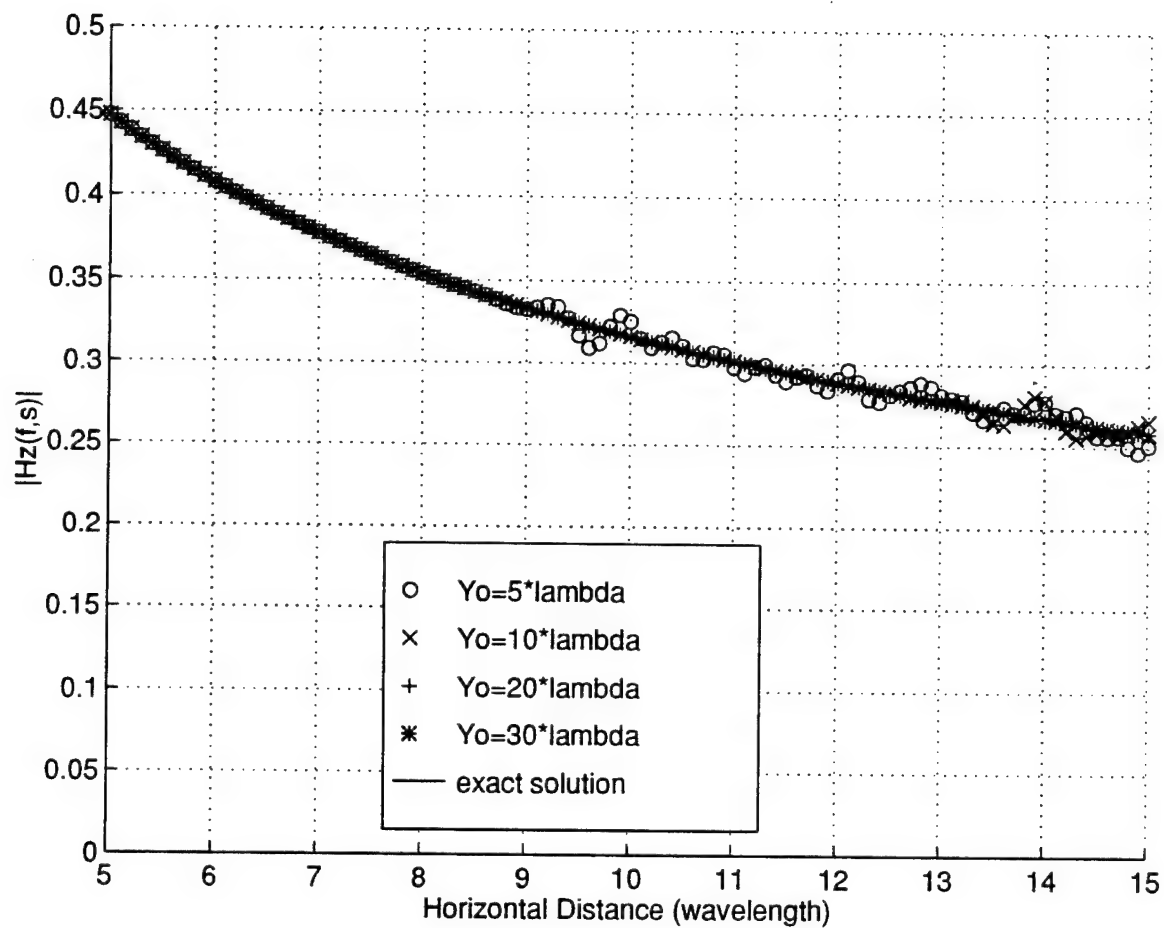
Figure 20.   Surface magnetic field versus distance.
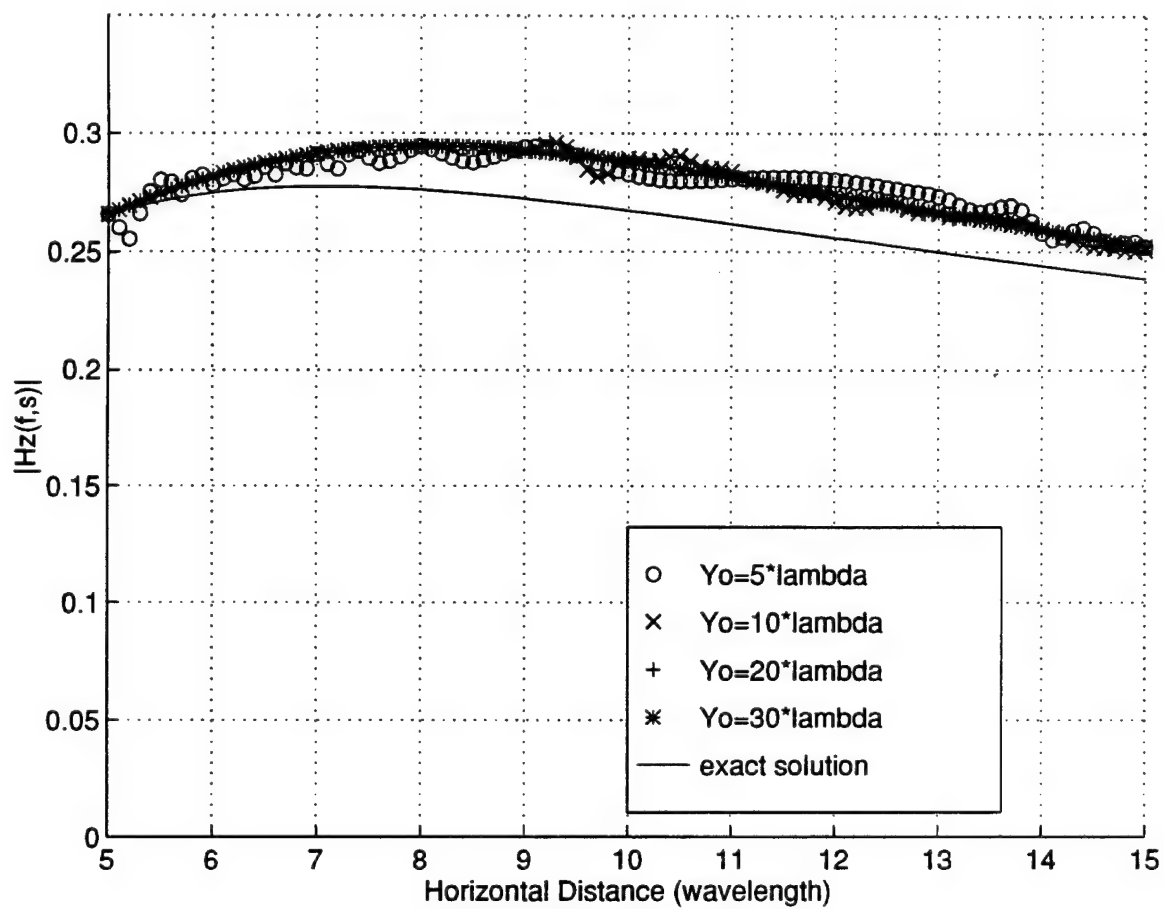
Figure 21. *Hz* versus distance @ height = 5λ.
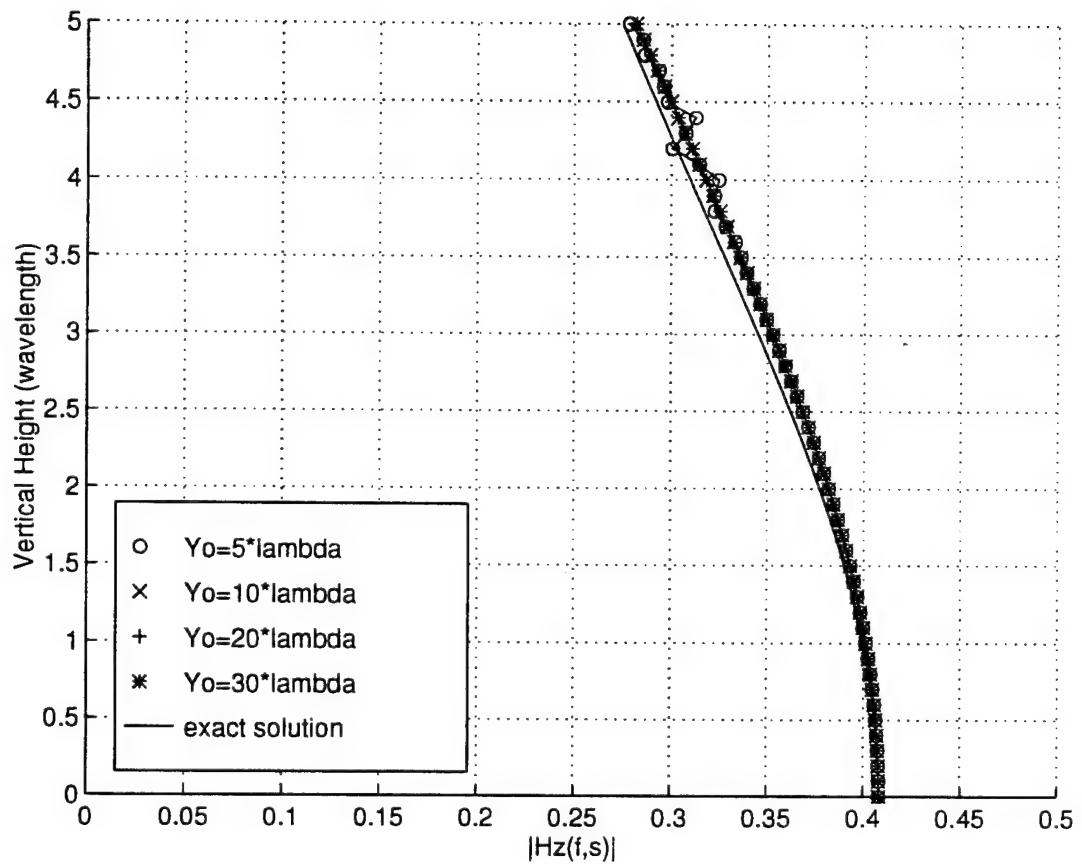
Figure 22. *Hz* versus height @ distance = 6λ.

42
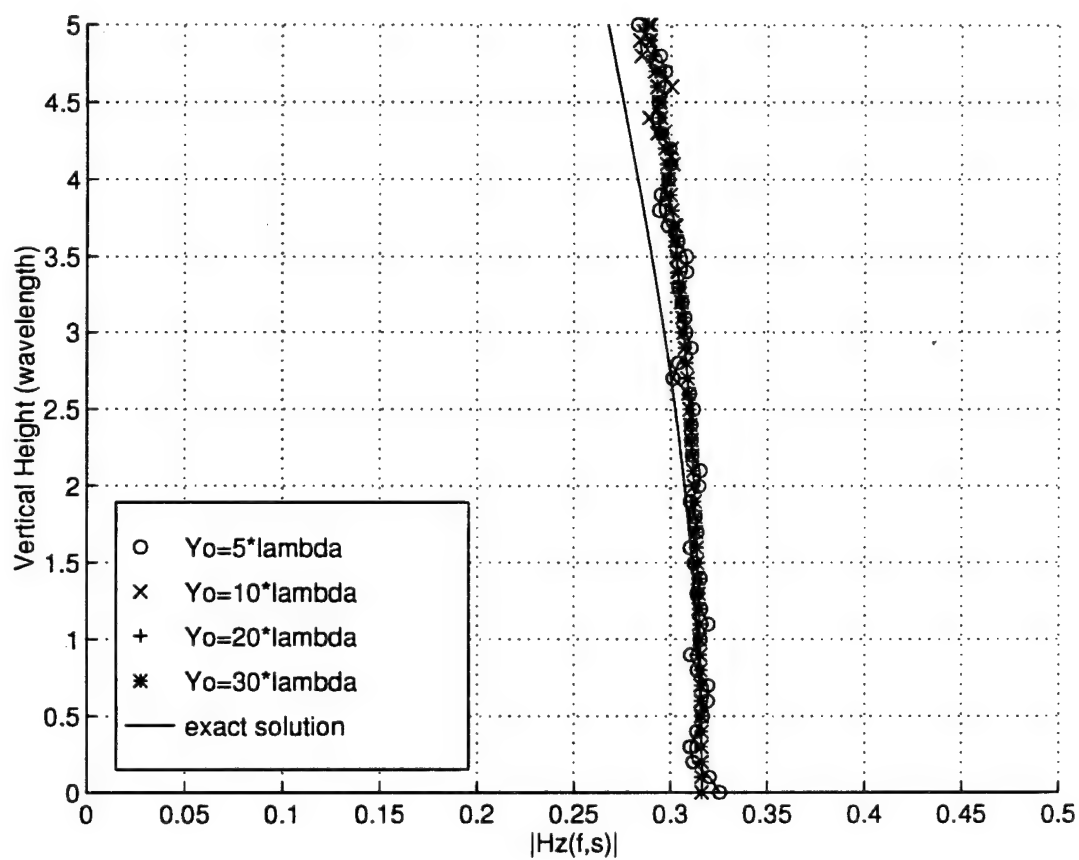
Figure 23. *Hz* versus height @ distance = 10λ.
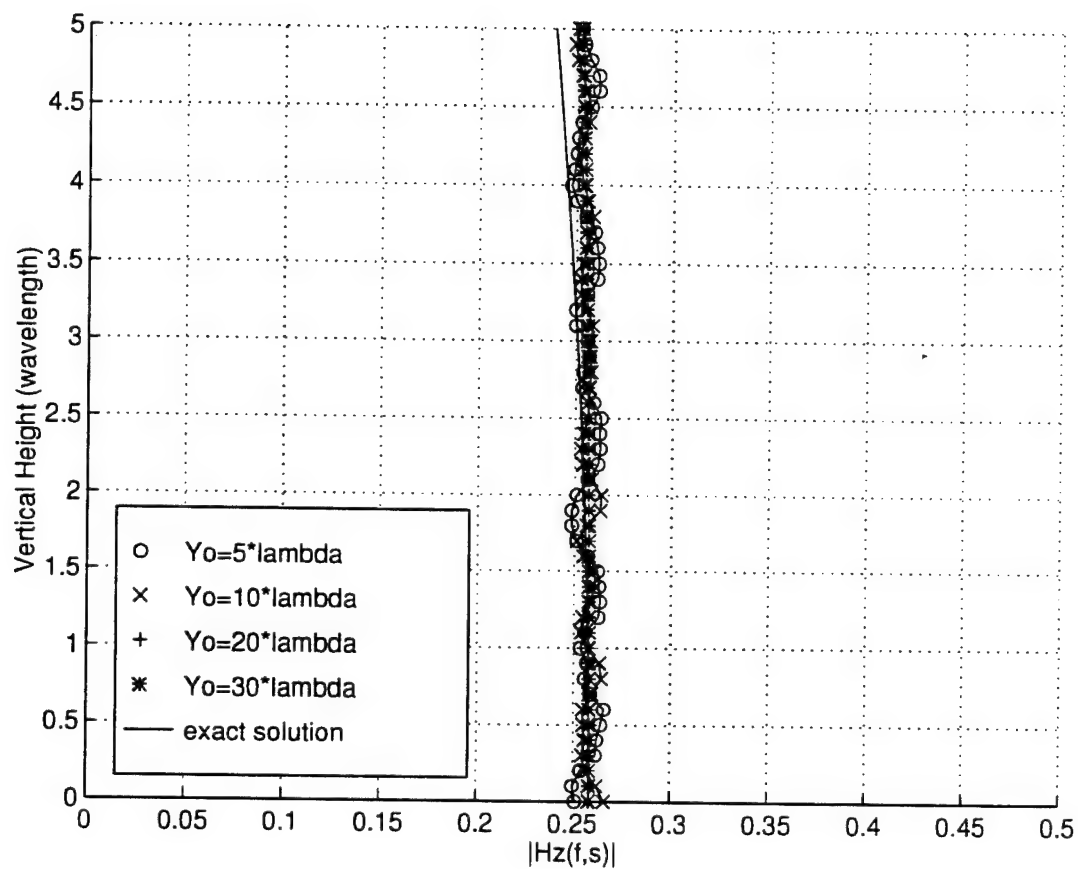
Figure 24. *Hz* versus height @ distance = 15λ.

44

C.   PROPAGATION OVER A PEC KNIFE-EDGE

Consider a perfectly conducting knife edge of height h_c as shown in Fig. 25, set on a perfectly conducting plane, with the transmitter and receiver both on the ground at distances d_1 and d_2. The attenuation factor, AF, at point B can be found analytically and is given by [Ref. 10]

$$AF = 4\sqrt{\frac{j}{2}} \int_{u_c}^{\infty} e^{-j\pi u^2/2} \, du, \tag{74}$$

where

$$u(\xi) = \xi\sqrt{\frac{2d}{\lambda d_1 d_2}}, \qquad u_c = u(\xi = h_c) = h_c\sqrt{\frac{2d}{\lambda d_1 d_2}}. \tag{75}$$
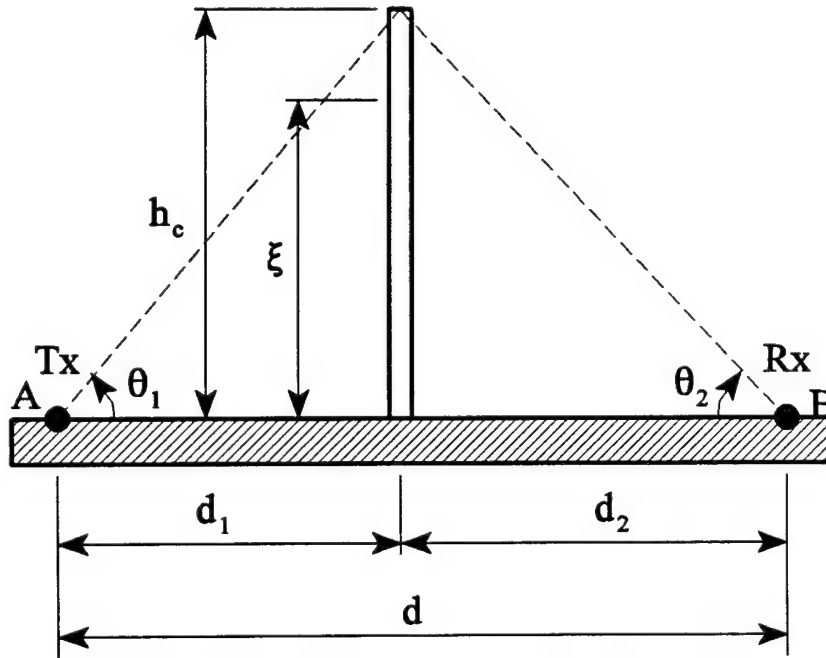
Figure 25.   Perfectly conducting knife edge between the transmitter at A and the receiver at B, both of which are on a perfectly conducting ground.

We consider the case where $h_c = 2\lambda$ and $d_1 = 10\lambda$. For this choice $\theta_1 = 11.3°$. A vertically polarized line source is placed at $x0 = 0$, $y0 = 0$ and the magnetic field is determined from an initial range of 5λ to a distance of 30λ. The height of the upper boundary is $y_o = 20\lambda$ and $y_{ubc} = y_o + 5\lambda$.

The variation of the surface magnetic field over the horizontal distance is plotted in Fig. 26. Variation of the magnetic field with height at a distance $d_2 = 2\lambda$ is plotted in Fig. 27. Comparison of the attenuation factors at $d_2 = 2\lambda$, 10λ, 15λ, and 20λ ($\theta_2 \approx 45°$, $11°$, $7.6°$, $5.7°$ respectively) computed numerically and the exact solution using Eq. (74) is given in Table 1.

Distance d_2	AF (Numerical)	AF (Exact)	Error (%)
2λ	0.7758	0.4071	90.57%
10λ	1.1674	0.6725	73.59%
15λ	0.9330	0.7250	28.69%
20λ	0.8048	0.7560	6.46%

Table 1. Attenuation factor for propagation over PEC knife edge.

The rather large oscillations seen near the surface in Fig. 27 could be due to the non-applicability of the parabolic equation for high angles (i.e., $\theta_2 > 15°$).

D.   PROPAGATION OVER A CIRCULAR BOSS IN A PEC PLANE

Next, we compare the numerical results for propagation over a semi-circular boss on a perfectly conducting plane. This problem typifies radiowave propagation over uneven terrain. A vertically polarized line source is placed in front of the semi-circular boss of radius $b = 0.5\lambda$ and centered at the origin. The transmitter is at $x0 = -0.75\lambda$, $y0 = 0.1\lambda$ from the origin and the initial data line is at -0.6λ from the center of the boss. There is good agreement between the exact solution given in [Ref. 9] and the numerical results generated here as evidenced in Fig. 28.
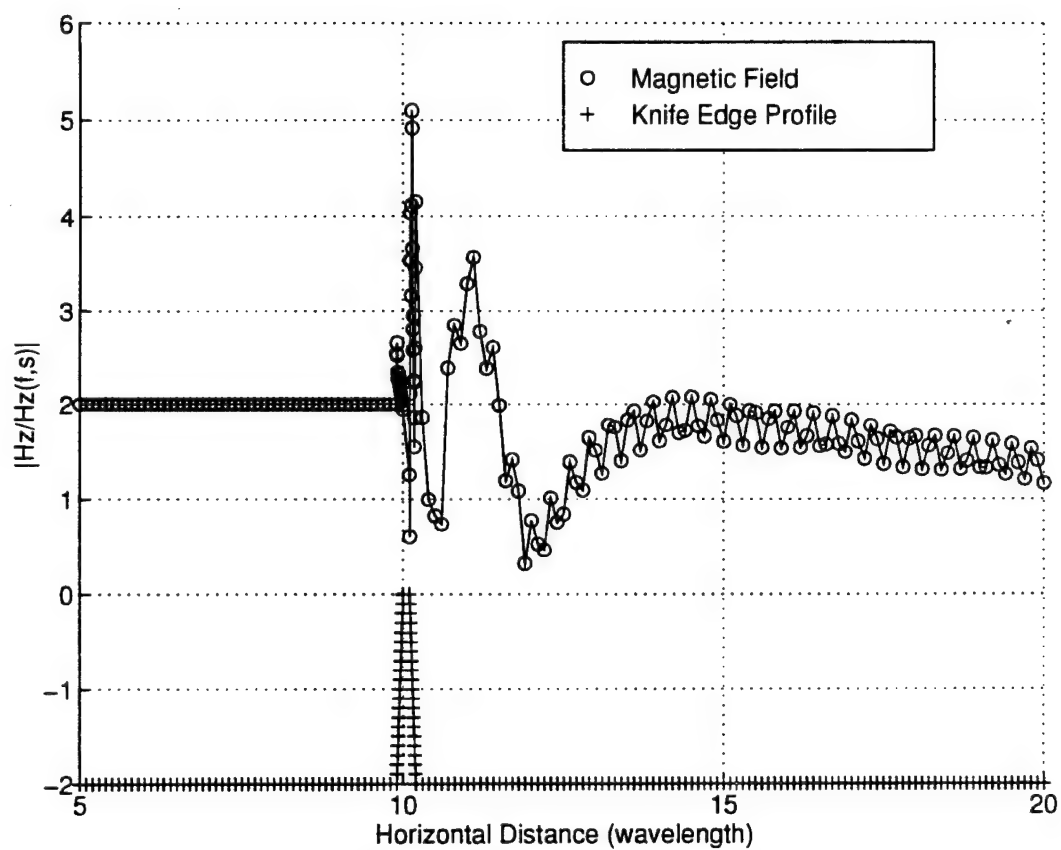
Figure 26.   Normalized surface magnetic field versus distance (PEC knife edge).

47
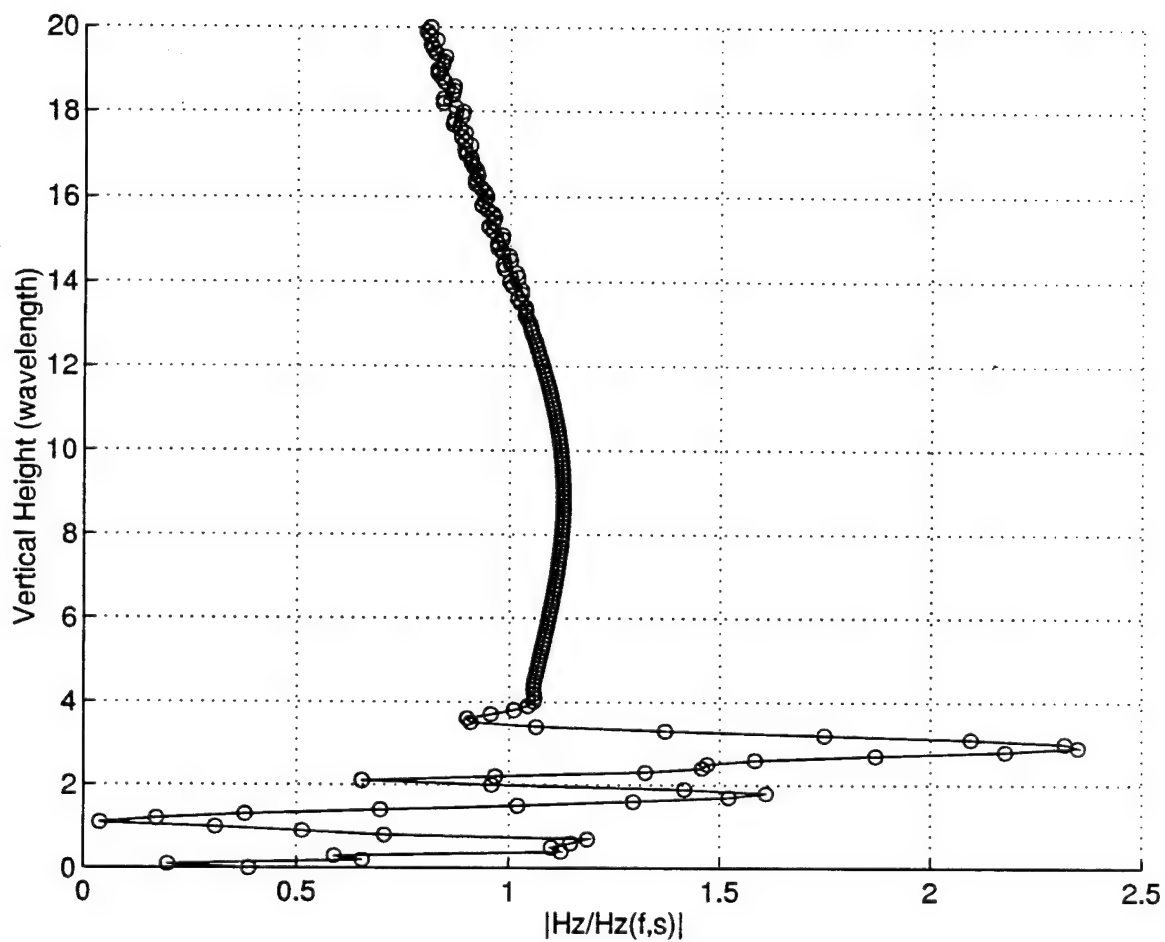
Figure 27.   Normalized magnetic field versus height @ $d2 = 2\lambda$ (PEC knife edge).

48
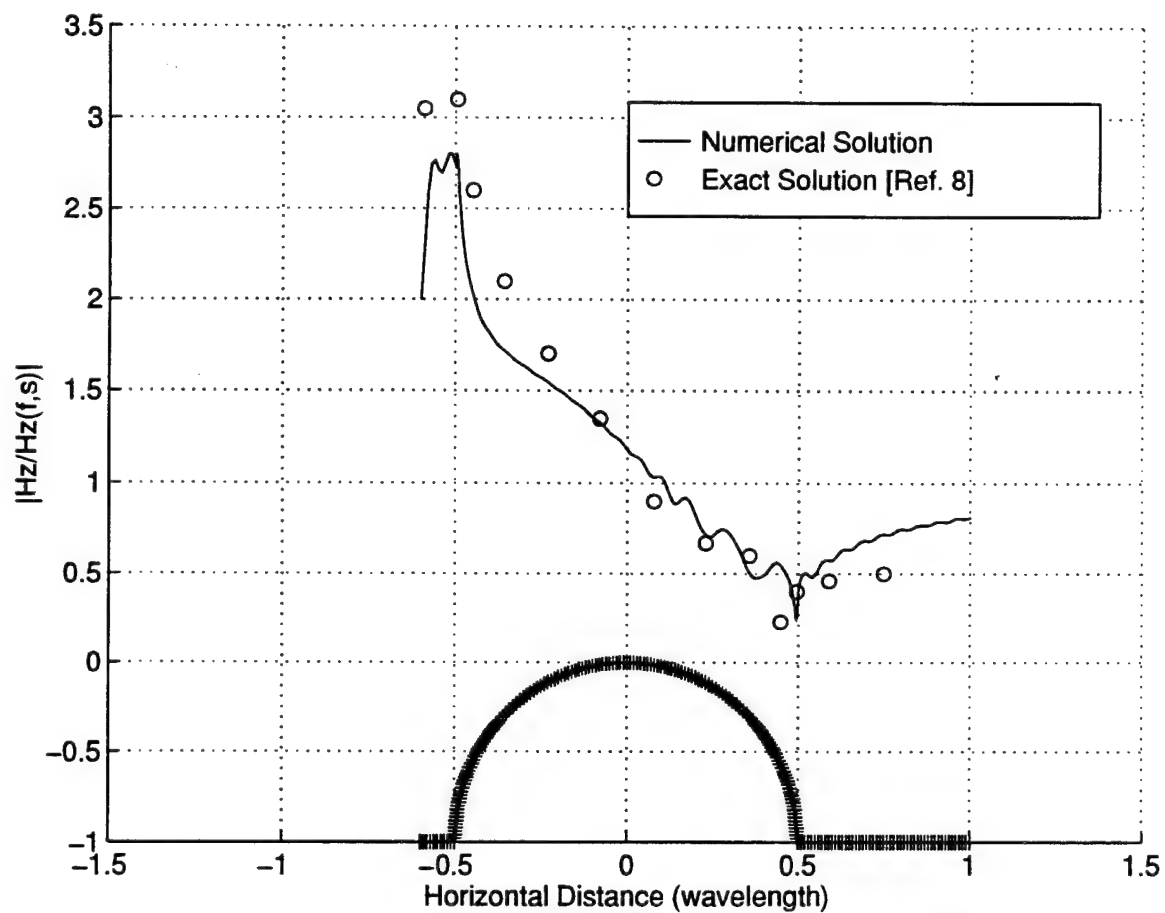
Figure 28. Magnitude of the normalized surface fields versus horizontal distance for a line source placed over a perfectly conducting plane with a semi-circular boss.

E.   PROPAGATION OVER A LOSSY IMPEDANCE PLANE

In the previous sections, we have considered only propagation over PEC surfaces. In this section, we will investigate the case of propagation over a lossy impedance plane. The ground constant chosen are $\epsilon_r = 10$, $\sigma_r = 180$ (corresponding to $\sigma = 10$ mS/m at 1 MHz). The line source is placed at $x0 = 0$, $y0 = 0.01\lambda$. The horizontal step size, $\Delta x = 0.1\lambda$, and the vertical step size, $\Delta y = 0.1\lambda$. The initial data line is 5λ away from the source, and the solution is allowed to propagate for 25 wavelengths. The magnetic field on the initial data line is generated from the fields on a flat lossy plane [Ref. 11]

$$H_z = -\frac{k_o}{4j}\left[\cos\theta_1 H_1^{(2)}(k_o r_1) + \cos\theta_2 H_1^{(2)}(k_o r_2) - j2\Delta_s\sqrt{\frac{2j}{\pi k_o r_2}}\frac{e^{-jk_o r_2}}{(\Delta_s + \sin\theta_2)}\right], \qquad (76)$$

where

$$r_1 = \sqrt{(x - x_o)^2 + (y - y_o)^2}, \qquad r_2 = \sqrt{(x - x_o)^2 + (y + y_o)^2},$$

$$\cos\theta_1 = \frac{(x - x_o)}{r_1}, \qquad \cos\theta_2 = \frac{(x - x_o)}{r_2}, \qquad \sin\theta_2 = \frac{(y + y_o)}{r_2}.$$

The results for the surface magnetic field are plotted in Fig. 29. Comparison is made with the data points for the exact solution given in Fig. 22, pp. 52 of [Ref. 9]. There is very good agreement between the numerical results and the exact solution.

F.   PROPAGATION OVER A LOSSY GAUSSIAN HILL

Next, we treat the case of propagation over a Gaussian shaped ridge or hill. The height $h(x)$ of the Gaussian hill is defined as

$$h(x) = He^{-9[(x-c)/w]^2}, \qquad (77)$$

where H is the maximum height, c is the location of the maximum, and w is a parameter controlling the width of the hill. A vertically polarized line source was placed at $x0 = 0$, $y0 = 0.01\lambda$ with $H = 1$ km, $c = 5$ km, and $w = 3$ km. The initial data line was at $x_{ini} = 2$ km.

50
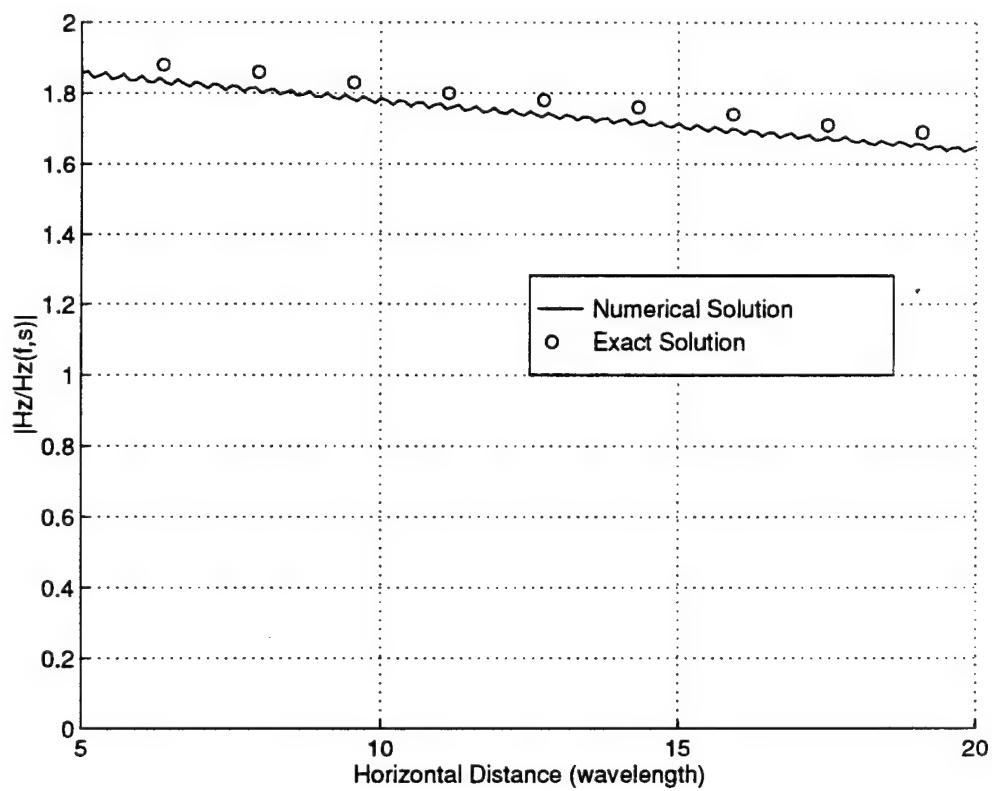
Figure 29.   Surface magnetic field versus distance (lossy plane).

51
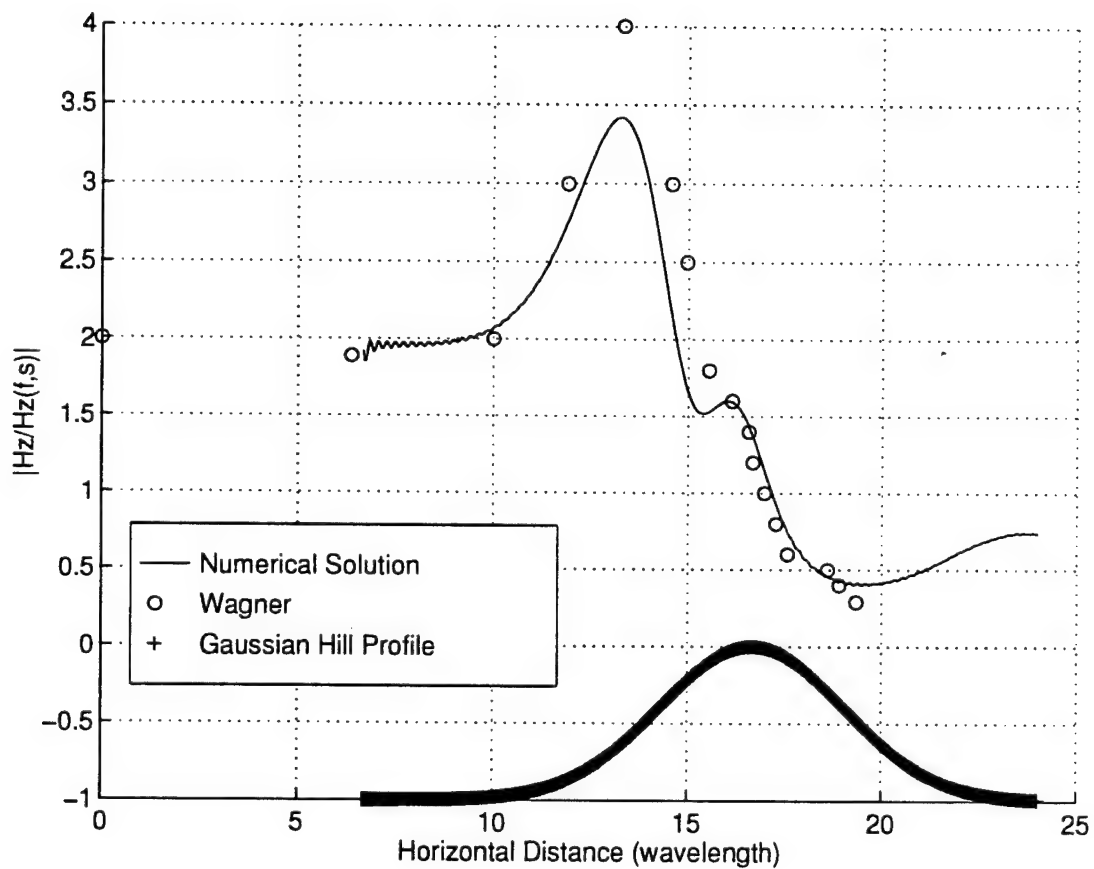
Figure 30. Magnitude of the normalized surface fields versus horizontal distance for a source placed at the origin in front of a Gaussian hill.

The ground constants were $\epsilon_r = 10$ and $\sigma_r = 180$ (corresponding to $\sigma = 10$ mS/m at 1 MHz). We plot the results of the normalized magnetic field in Fig. 30 together with the results generated from WAGNER [Ref. 12]. Although there is minor differences in the magnitude of the normalized magnetic field, it is seen that the trend in the two results are in good agreement. Both results predict large peak around 3.9 km from the source, which is attributed to focusing by the concave surface of the hill. A secondary peak at 4.5 km is also predicted by the numerical method.

G.   PROPAGATION OVER A PEC ISOSCELES HILL

Experimental results for propagation over a PEC isosceles triangular hill are given in [Ref. 10]. In [Ref. 10], an irregular path consisting of an isosceles hill of height 1.23λ was constructed from aluminum sheets whose surface impedance was taken to be zero. The dimensions of the sloping side of the hill are shown in Fig. 31.
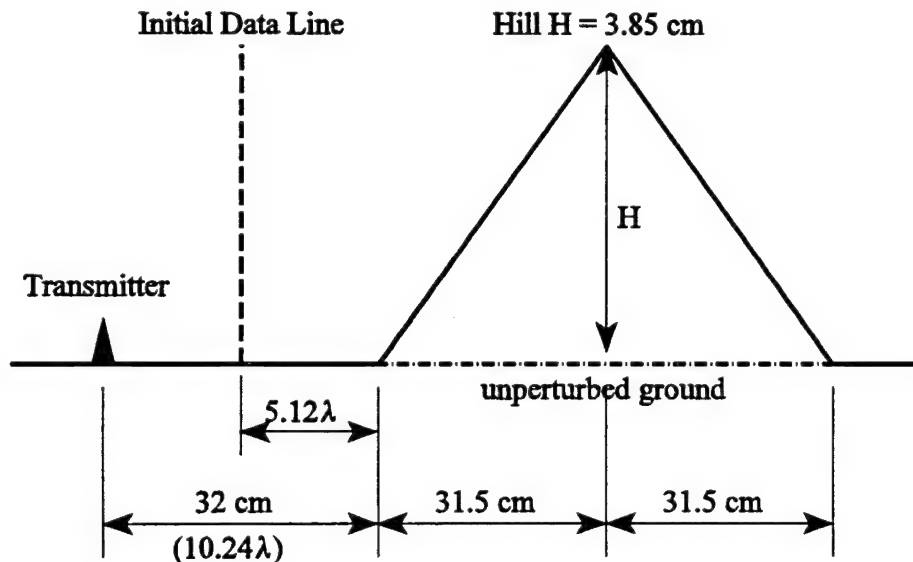
Figure 31.   Perfectly conducting isosceles triangular hill of height 1.23λ and baselength 20.16λ.
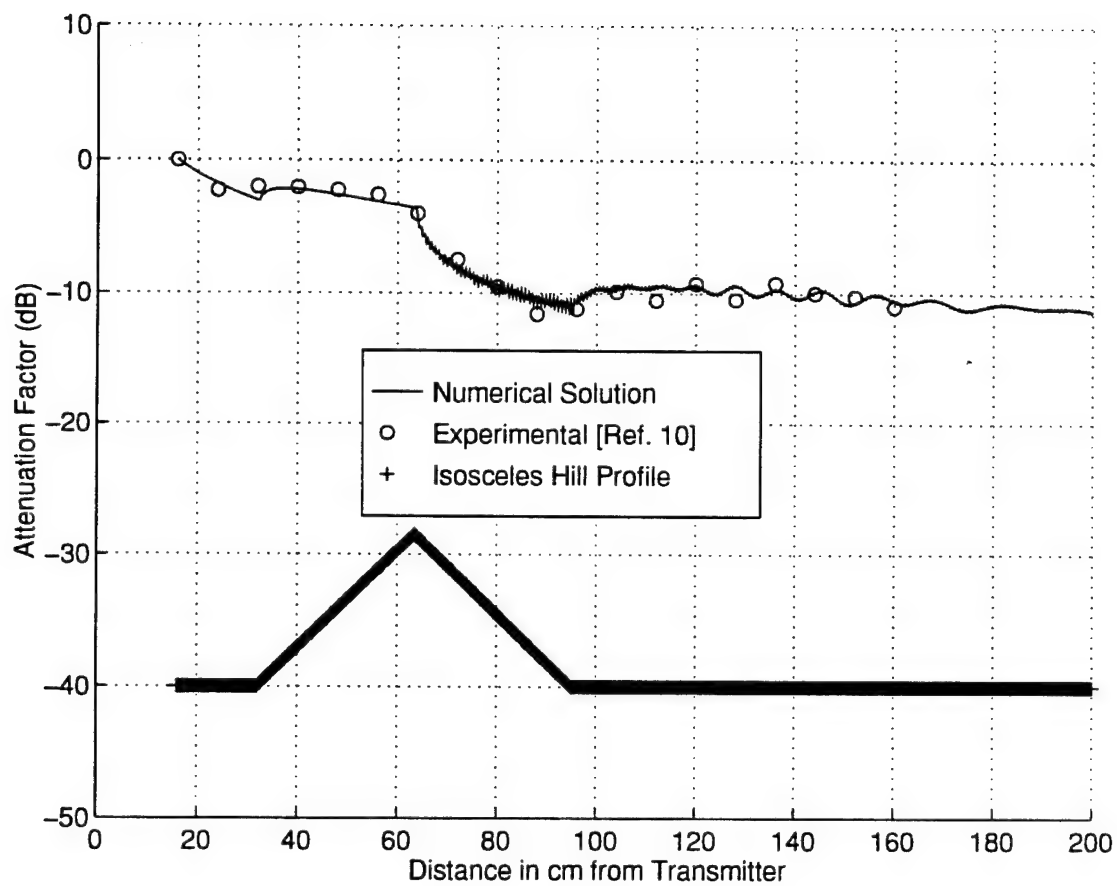
Figure 32. Magnitude of the normalized fields across a perfectly conducting isosceles triangular hill.

54

Using the vertical line sources at a distance of 10.24λ from the beginning of the hill, and a frequency of 9.6 GHz, the numerical solution is computed and marched from an initial data line of 5.12λ. The normalized magnetic field taken at a height $h_R = 0.16\lambda$ above the irregular surface is plotted in Fig. 32. We have computed the attenuation factor for the experimental values given in Fig. 4, pp. 39 of [Ref. 10] as follows

$$AF(dB) = 20\log\left(\frac{E(r)}{E(r_i)}\right) + 10\log\left(\frac{r}{r_i}\right) ,$$
(78)

and compared them to the results obtained from our numerical method. In our case, we have chosen $r_i = 5.12\lambda$ to coincide with the initial data line. It can be seen that there is excellent agreement between the experimental data and the results from the numerical solution.

H.   PROPAGATION OVER A PEC CLIFF

Measured data for the magnitude of the field strength over an aluminum cliff edge was also given in [Ref. 10]. Measurements were carried out over the aluminum cliff which was situated 10.24λ from the transmitter and of height 1.05λ as shown in Fig. 33.
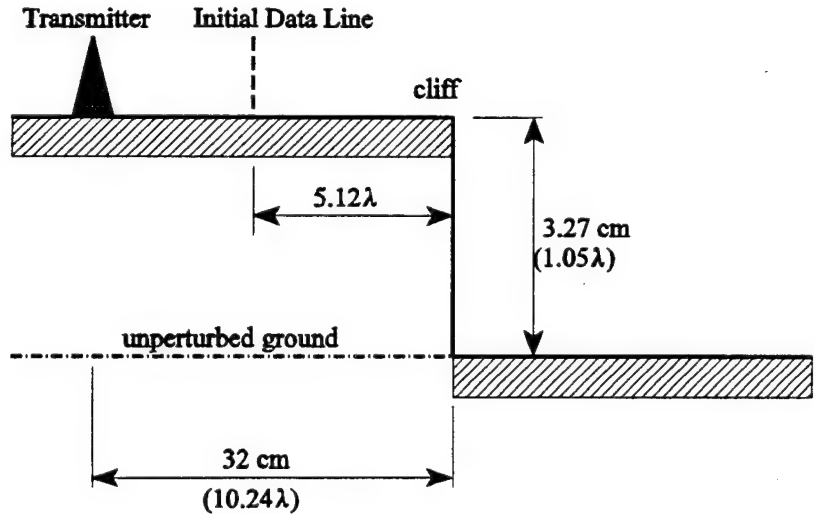
Figure 33.   Perfectly conducting cliff edge of height 1.05λ.

We set up our computation model based on the geometry given in Fig. 33. At a frequency = 9.6 GHz, we placed a vertical line source at 10.24λ from the edge of the cliff, and set the initial data line at 5.12λ. We have chosen $\Delta x = \Delta y = 0.08\lambda$ (instead of $\Delta x = \Delta y = 0.1\lambda$) to enable plotting of data at a height, $h_R = 0.16\lambda$ (2 vertical steps) at which height the measurements were also taken. The result of the numerical solution is plotted in Fig. 34. From the plot, we observe that the field attenuates over the first flat section as if the cliff is were absent. Immediately beyond the cliff, however, the field strength drops suddenly in the shadow region, and then increases with further increase in range, before returning as before to decreasing values with increased range. We have computed the attenuation factor based on the measured data given in Fig. 6, pp. 39 of [Ref. 10] using Eq. (78) and superimposed them in Fig. 34. Again, there is excellent agreement between the numerical solution and the experimental results, even for points near the cliff edge and immediately beyond the cliff.

I. PROPAGATION OVER A DIELECTRIC COATED CLIFF

Experimental results were also available for a dielectric coated cliff [Ref.10]. Measurement have been carried out over the same cliff edge given in Fig. 33, but with the horizontal surfaces constructed from polypropylene covered aluminum sheet and the vertical edge made of aluminum sheet alone. The normalized surface impedance of the polypropylene-covered sheet with $\epsilon_r = 2.2$ and dielectric thickness, can be calculated to be $\Delta_s^H = j0.171$, which is highly inductive. We use the same computational model as in Section H and plot the results in Fig. 35. Again, we compute the attenuation factor based on the measured data given in Fig. 7, pp. 40 of [Ref. 10] using Eq. (78) and superimposed it in Fig. 35. Again, we observe very good agreement between the magnitude of the of the attenuation factor between the numerical solution and the measured value. This is true for points near the cliff edge and immediately beyond the cliff edge. The behavior of the field strength computed numerically also corresponds very well with the experimental results. The results in Sections H and I clearly demonstrated the versatility of this numerical method for terrain with PEC surface and dielectric coated surface.
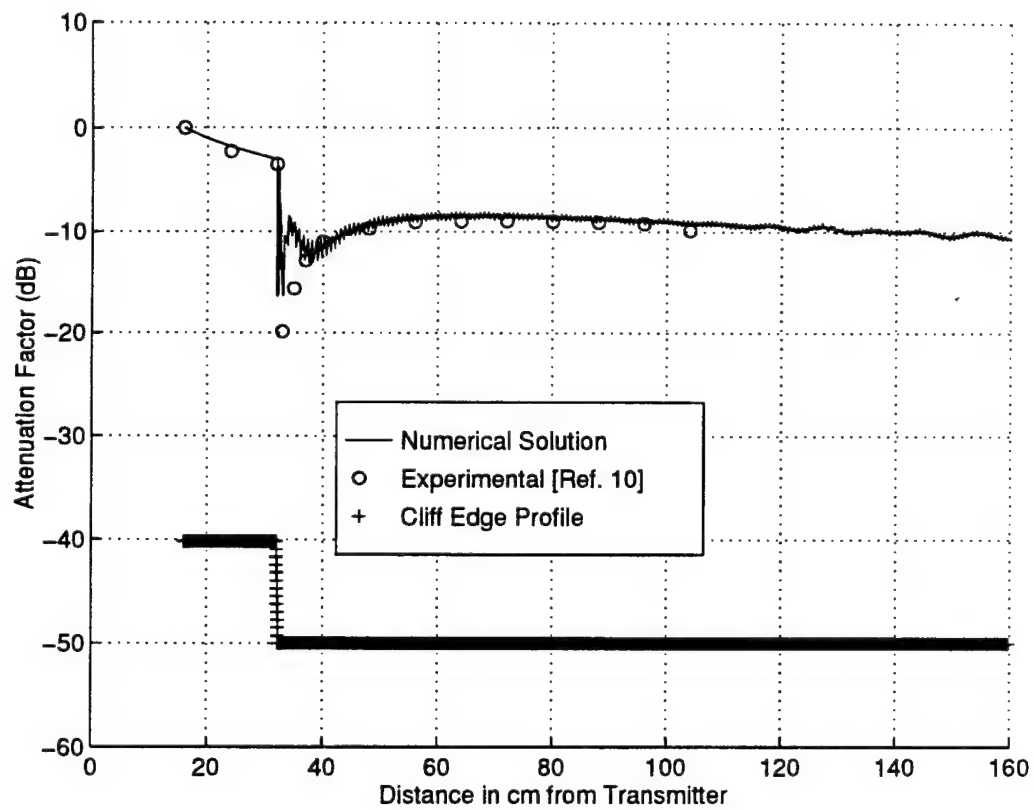
Figure 34. Magnitude of the normalized fields across a perfectly conducting cliff.
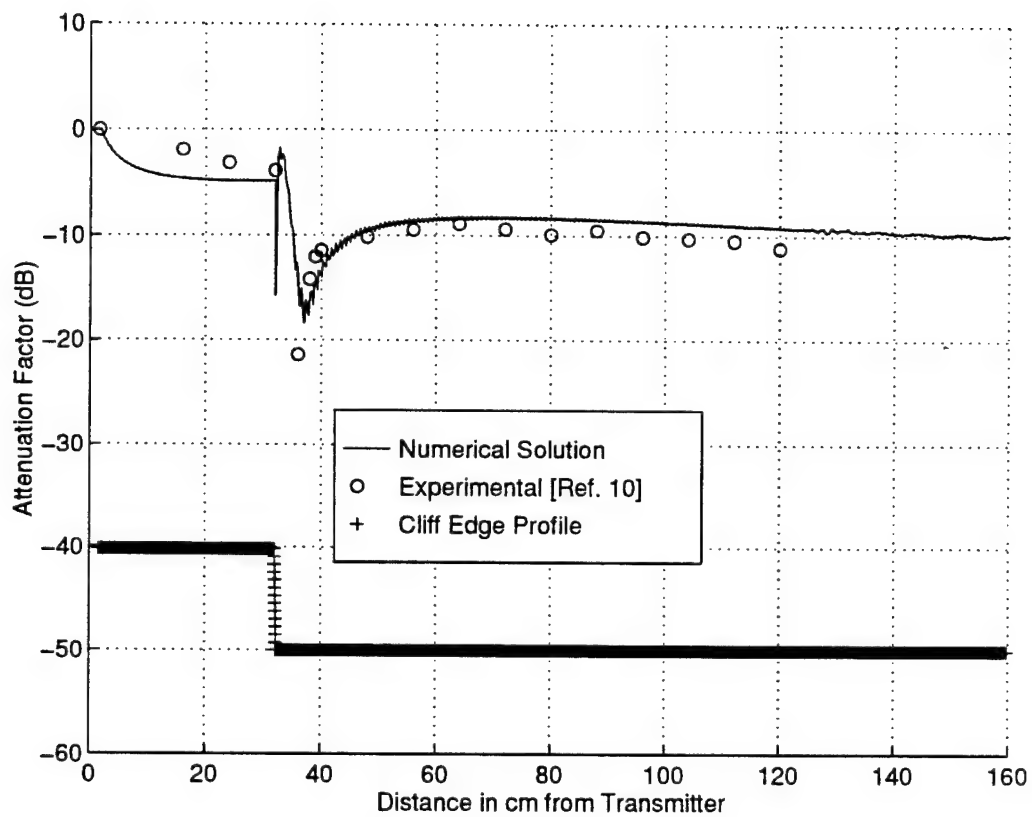
Figure 35. Magnitude of the normalized fields across dielectric coated horizontal surfaces on a cliff edge; $\epsilon_r = 2.2$. Dielectric thickness 0.15 cm. Normalized surface impedance is j0.171.

58

J.   PROPAGATION OVER A MIXED PATH (LAND-SEA-LAND)

Next, we would like to examine the capability of the parabolic equation formulation to predict radiowave propagation over long range and inhomogeneous ground. Consider a four-thirds earth atmosphere over a ground with electrical properties that change along the propagation path. The initial and final portions of this "mixed-path" problem are over land (ϵ_r = 15, σ = 0.03 mho/m), while from 47 to 50 km from the source the propagation takes place over sea (ϵ_r = 80, σ = 4 mho/m). Results of path-loss predictions at a receiver height z_r = 5 m for a 59.7 MHz transmitter at a height of z_t = 5 m using IFDG method with y_o = 10m, x_{ini} = 40 km, Δy = 1m, and Δx = 100 m for range, $r < 47$ km and $r > 52$ km, Δx = 10 m for 47 km $< r < 50$ km; and Δx = 1 m for 50 km $< r < 52$ km is available in [Ref. 1] and the Millington approximation in [Ref. 13]. We computed our numerical solution based on the geometry described in [Ref. 1]. In view of the large distance, the asymptotic form of Hankel function was used in Eq. (76) to compute the magnetic field at the initial range

$$H_1^{(2)}(\tilde{R}) \approx \sqrt{\frac{2}{\pi\tilde{R}}}\ e^{-j\tilde{R} - 3\pi/4}\ , \tag{79}$$

where $\tilde{R} \approx |k_o(x-x_o)|$. The path loss is computed as

$$L = -20\ \log_{10}\left(\frac{Hz}{\sqrt{r}}\ \frac{\sqrt{\pi}}{k_o^2}\right)\quad (dB), \tag{80}$$

and plotted in Fig. 36. We see that there is excellent agreement in the path loss (attenuation factor) between our computed results and the those computed using the IFDG method [Ref. 1]. We also noticed that the general behavior of our numerical solution is identical to the prediction given in [Ref. 1].

K.   PROPAGATION OVER A LOSSY VALLEY

We also investigate the capability of the parabolic equation formulation to predict radiowave propagation over a lossy valley. Consider a vertical source radiating on a smooth horizontal ground at a distance 30 km from the edge of a 100-m-deep valley that is symmetric

about the midpoint of its horizontal bottom, which is 1 km long. The slope of each wall is $\pm 1/10$, so that the total horizontal length of the terrain irregularity is 3 km. The ground is characterized by $\epsilon_r = 4$, $\sigma = 0.001$ mho/m. Results using the IFDG prediction and the WAGNER method [Ref. 12] for receiver on the ground are given in [Ref. 1]. In [Ref. 1], the IFDG results were obtained using $x_{ini} = 25$ km, $\Delta y = 1$m, $\Delta x = 20$ m for all range, r, except for 30 km $< r <$ 35 km for which $\Delta x = 1$ m. Again, our computational geometry is similar to the IFDG geometry. The initial field is computed using Eq. (76) with the asymptotic form for Hankel function given in Eq. (79). The path loss for propagation at a frequency of 10 MHz is computed using Eq. (80) and plotted in Fig. 37. Although there is a slight deviation in the path loss between our numerical results and the IFDG method [Ref.1], we notice that the general trend of the path loss between our method and the IFDG method remains identical. The deviation in the magnitude of the path loss could be due to the fact that [Ref. 12] has considered an azimuthally symmetrical profile while our profile is 2-dimensional and laterally symmetrical.
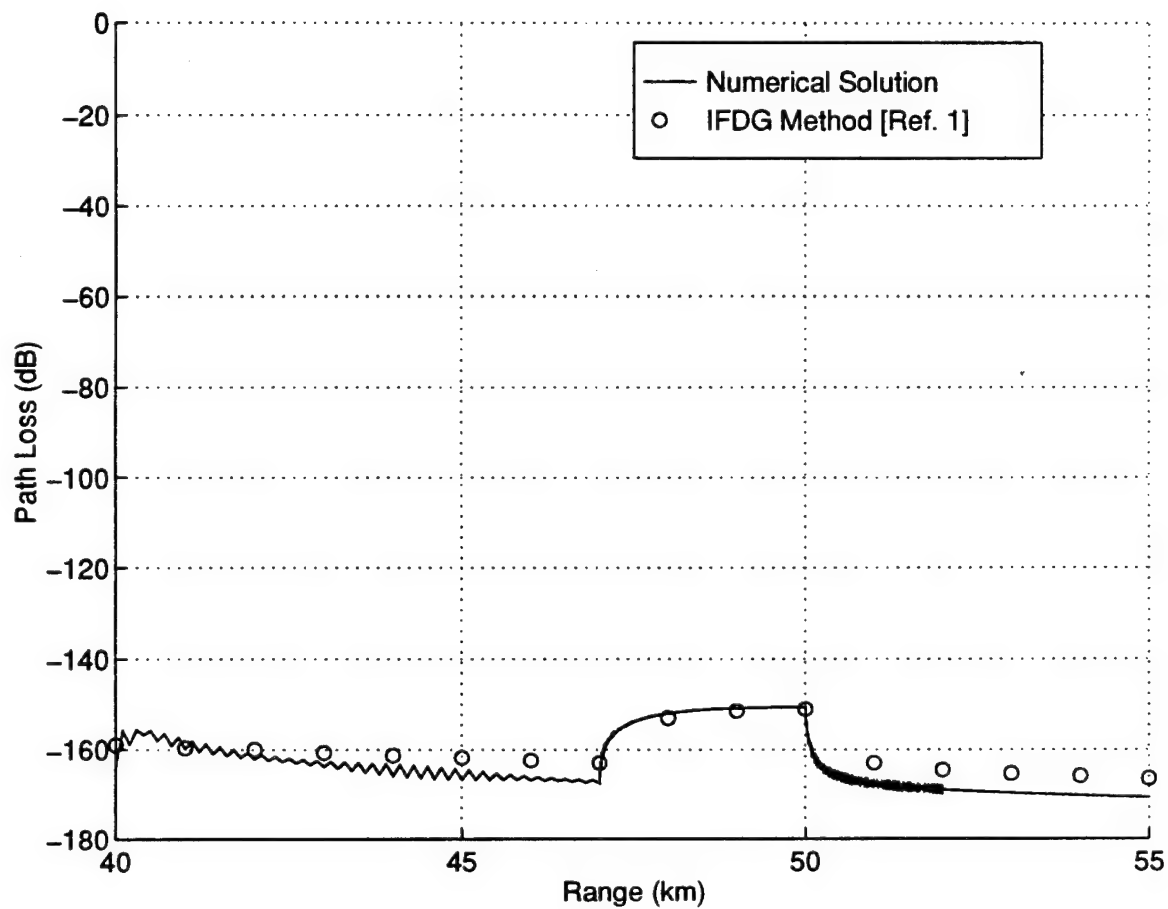
Figure 36.   Path loss over a land-sea-land path, f = 59.7 MHz, transmitter at 5m, receiver at 5m, vertical polarization.
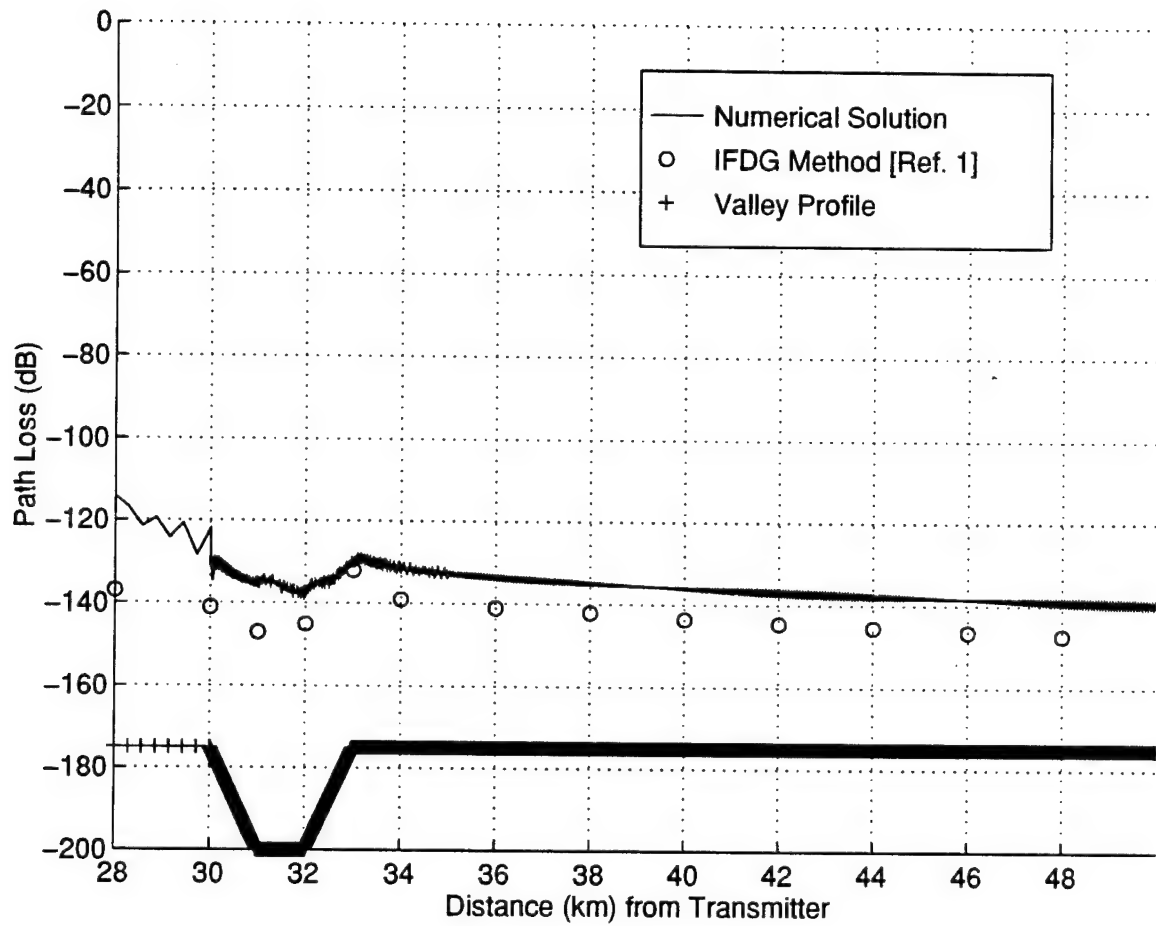
Figure 37. Path loss for propagation over a valley, $f = 10$ MHz, transmitter and receiver on the ground.

V. CONCLUSIONS AND RECOMMENDATIONS

In this thesis, a numerically efficient method to model tropospheric radiowave propagation over irregular terrain was implemented and tested. The parabolic equation method was used for predicting radiowave propagation. A tropospheric boundary condition was used to truncate the computational domain at the top, while an impedance boundary condition was used on the uneven terrain to characterize the ground. Because the parabolic equation method is a full-wave method, it includes all aspects of wave propagation such as forward reflection, refraction, diffraction, and surface wave propagation. However, it ignores back-scattering. Since the parabolic equation method models wave propagation only in the forward direction, it allows for a rapid solution of the fields by way of marching along in range starting from an initial range. A great advantage of the parabolic equation method compared to the commonly used ray method is that it is valid in the shadow region where the latter method completely breaks down. Furthermore, it appears to be the only practical method for predicting propagation over long ranges (thousands of wavelengths) and over a wideband (HF through SHF).

The main advancement made in this thesis is the use of a non-rectangular mesh in a curvilinear coordinate system to model the uneven terrain. A body fitted coordinate is generated based on the specification of the ground profile, and the parabolic PDE, together with the boundary conditions, are cast in a curvilinear coordinate system. This not only makes the method more efficient, but also permits more accurate imposition and modeling of the boundary conditions. We used the Crank-Nicolson implicit scheme in the computational domain to solve the parabolic PDE. For a cartesian grid, this method is convergent and stable for all finite values of step size. In this method, the parabolic PDE is considered as being satisfied at the mid-point of the computational grid. Central difference approximations, which are second-order accurate, are used in the interior as well as at the boundaries.

Numerical results to predict radiowave propagation over various obstacles were computed and validated with the results available in the open literature. These include both

63

a PEC plane and impedance ground with differing permittivity and conductivity. Excellent agreement was observed and demonstrated for the following cases : a PEC circular boss, lossy Gaussian hill, PEC triangular hill, loaded and unloaded cliff edges, mixed path, and a lossy valley. Three-dimensional obstacles are outside the scope of this thesis.

The model presented in this thesis can be applied to problems in short range communications or radar target detection. At HF/VHF frequencies, the antennas are electrically close to the ground leading to significant perturbation of the received signals. Assessment of propagation of HF/VHF signals over inhomogeneous and irregular terrain is highly desirable. In the case of a radar system, signals received from a target depend on the direct ray and a ground reflected ray. The path taken by the ground reflected ray depends on the terrain roughness and ground constants. Since target detection is based on the composite signal, it is important to assess ground conditions and atmospheric factors. The numerical model developed in this thesis provides a useful tool for predicting the performance of radar or communication links before commencing to design, develop, and deploy the system in the field. From the model developed, one can predict propagation factors such as path loss, coverage diagrams, and the perturbation of antenna radiation patterns over realistic terrains and ranges.

This thesis represents the beginning of an effort to predict radiowave propagation using the parabolic equation method. In its standard form, the accuracy of the method is limited to waves traveling within $\pm 15°$ from the horizontal. It is recommended that follow-on work should use a wide-angle parabolic equation method to accommodate waves traveling over wider angles and in an inhomogeneous atmosphere.

APPENDIX A.   MATLAB SOURCE LISTINGS

The formulation described in Chapter II and the numerical procedure described in Chapter III were implemented using MATLAB sofware. The routines that generated the results in Chapter IV are listed below.

A.   EXECUTIVE ROUTINE

```
% Filename : main.m
% Title : Main Program or Executive Program
% Revision No. : R1.0
% Date of Last Revision : 10 Mar 95
% Comments :
%        This is the main program for computing the Parabolic
%        Equation Solution of Radiowave Propagation in an
%        Inhomogenous Atmosphere and Over Irregular Terrain.
%
% Input Variables : none
%
% Output Variables :
%        xphy           : x-coordinate of physical domain
%        yphy           : y-coordinate of physical domain
%        U              : computed Hz-Field
%        wavelength     : wavelength (frequency/3e8)
%        time           : total CPU time used
%
% Associated Matlab Files :
%        Called by      : none
%        Subroutines    : data
%                         dinp
%                         cmet
%                         hfld        '
%                         epde
%
% Associated Functions   : none
%
clear all;
t=cputime;                  % start CPU clock
data                        % input data file
dinp                        % compute the physical domain
cmet                        % compute the metric
hfld                        % compute Hz-Field on initial data line
epde                        % march and compute Hz-Field
time=cputime-t;
save output xphy yphy N M U time wavelength;
```

B. PHYSICAL DOMAIN GRID

```
% Filename : dinp.m
% Title : Computation of Physical Domain
% Revision No. : R1.0
% Date of Last Revision : 10 Mar 95
% Comments :
%        This subroutine computes the entire computational
%        domain based on the user input data for the physical
%        ground plane.
%
% Input Variables :
%        xin              : x-coordinate of ground plane
%        yin              : y-coordinate of ground plane
%
% Output Variables :
%        xphy             : x-coordinate of physical domain
%        yphy             : y-coordinate of physical domain
%
% Associated Matlab Files :
%        Called by        : main
%        Subroutines      : none
%
% Associated Functions    : none
%
nseg=length(xin)-1;        % total number of segment
%
%%%%% Compute horizontal axis of the physical domain %%%%%
%
st=1;
for i=1:nseg;
  npts(i)=round(sqrt((xin(i+1)-xin(i))^2+(yin(i+1)-yin(i))^2)/xdel);
  xphy(st)=xin(i);
  yphy(st)=yin(i);
  for j=1:npts(i)-1;
    xphy(st+j)=xin(i)+j*(xin(i+1)-xin(i))/npts(i);
    yphy(1,st+j)=yin(i)+j*(yin(i+1)-yin(i))/npts(i);
  end;
  st=st+npts(i);
end;
xphy(st)=xin(length(xin));  % include the last point for x
yphy(st)=yin(length(yin));  % include the last point for y
%
%%%%% Compute vertical axis of the physical domain %%%%%
%
M=length(xphy)-1;
N=round(yup/ydel);
for i=1:N;
  yphy(i+1,:)=(1-i/N).*yphy(1,:)+(i/N)*yup;
end;
```

C.   CURVILINEAR COORDINATE SYSTEM METRIC

```
% Filename : cmet.m
% Title : Generation of Curvilinear Coordinate System Metric
% Revision No. : R1.0
% Date of Last Revision : 10 Mar 95
% Comments :
%        This subroutine computes the various metrics or derivatives
%        (dx_xi, dx_eta, dy_xi, dy_eta, ddy_eta) at any interior
%        points. In the Crank Nicolson implicit scheme, the metrics
%        are needed at the midpoint with respect to xi, i.e., at
%        xi=xi+del_xi/2.
%
% Input Variables :
%        xphy                : x-coordinate of physical domain
%        yphy                : y-coordinate of physical domain
%
% Output Variables :
%        dx_xi               : 1st order x-derivative w.r.t. xi
%        dx_eta              : 1st order x-derivative w.r.t. eta
%        dy_xi               : 1st order y-derivative w.r.t. xi
%        dy_eta              : 1st order y-derivative w.r.t. eta
%        ddy_eta             : 2nd order y-derivative w.r.t. eta
%
% Associated Matlab Files :
%        Called by          : main
%        Subroutines        : none
%
% Associated Functions      : none
%
msize=ones(size(yphy(:,1)));
dx_xi=msize*(xphy(2:M+1)-xphy(1:M));
dx_eta=0;
for i=1:N+1;
  dy_xi(i,1:M)=(1-(i-1)/N).*(yphy(i,2:M+1)-yphy(i,1:M));
end;
dy_eta=msize*((yphy(N+1,1)-(yphy(1,2:M+1)+yphy(1,1:M))./2)./N);
ddy_eta=0;
```

D.   MAGNETIC FIELD ON INITIAL DATA LINE

```
% Filename : hfld.m
% Title : Generation of Hz-Field on Initial Data Line
% Revision No. : R1.0
% Date of Last Revision : 10 Mar 95
% Comments :
%        This subroutine generates the magneic field (Hz-Field)
%        at the initial data line for a line source over
%        an impedance plane.
%        (Note : Never place the initial data line at the
```

67

```
%            same location as the transmitter, else the field
%            generated would be zero).
%
% Input Variables :
%        yphy                : y-coordinate of physical domain
%
% Output Variables :
%        Hz                  : Magnetic Field @ initial data line
%
% Associated Matlab Files :
%        Called by       : main
%        Subroutines     : none
%
% Associated Functions : hankel2
%
yinit=[yphy(1:N,1)' yphy(N+1,1):ydel:ytop];
Ro=sqrt((xphy(1)-x0).^2+(yinit-y0).^2)*ko;
%
%%%%% Generate Hz-Field using Fredholm Equation %%%%%
%
hr2=hankel2(0,Ro);                      % load Hankel function of 2nd order
H=2*((1j*ko)/4).*((xphy(1)-x0)./Ro).*hr2;
Hz=H.';
%
% Note:  "." is for Nonconjugated Transpose. Using only "'"
%        will result in conjugated transpose (i.e. the sign
%        of the complex term is inverted)
```

E.   FORMULATION OF PARABOLIC EQUATION MATRIX

```
% Filename : epde.m
% Title : Matrix Equation for the Parabolic System Equations
% Revision No. : R1.0
% Date of Last Revision : 10 Mar 95
% Comments :
%        This program defines the PDE for the matrix equations
%        and performs the numerical implementation using the
%        Crank-Nicolson Implicit Scheme (Discretization).
%        The applicability of the PDE equation is also
%        extended to accommodate the derivative boundary
%        conditions on the lower and upper boundaries.
%
% Input Variables :
%        dx_xi           : 1st order x-derivative w.r.t. xi
%        dx_eta          : 1st order x-derivative w.r.t. eta
%        dy_xi           : 1st order y-derivative w.r.t. xi
%        dy_eta          : 1st order y-derivative w.r.t. eta
%        ddy_eta         : 2nd order y-derivative w.r.t. eta
%        Hz              : Magnetic Field @ initial data line
%
```

```matlab
% Output Variables :
%        U                : computed Hz-Field
%
% Associated Matlab Files :
%        Called by        : main
%        Subroutines      : elbc
%                           eubc
%
% Associated Functions    : none
%
%%%%% Assume constant atmospheric refractive index %%%%%
n=1; dn_x=0; dn_y=0;
a1=-(2/n)*dn_x; a2=-(2/n)*dn_y;
a1_star=(n^2-1-2j*(a1/ko))*(ko^2);
%
%%%%% Set up the matrix coefficients, (M x N) for b1, b2, b3 %%%%%
%
temp1=2j*ko-a1;
b1=dx_xi.*a1_star./temp1;
b2=dx_xi./dy_eta.*((a2-ddy_eta./dy_eta.^2)./temp1+dy_xi./dx_xi);
b3=dx_xi./(temp1.*dy_eta.^2);
alpha=0.5.*(b3+0.5.*b2);
beta=(b3-0.5.*b1);
gamma=0.5.*(b3-0.5.*b2);
%
%%%%% Initialization of Magnetic Field %%%%%
%
U(1:N+1,1)=Hz(1:N+1);
%
%%%%% Compute coefficient of Lower BC %%%%%
%
elbc
%
%%%%% Compute invariant coefficient of Upper BC %%%%%
%
r(1:M)=sqrt((8j*ko)/pi)./sqrt((xphy(2:M+1)-xphy(1:M))./2);
%
%%%%% Loading the matrix %%%%%
%
for p=1:M;
 A=spdiags([gamma(:,p) -(1+beta(:,p)) alpha(:,p)], -1:1, N+1, N+1);
 B=spdiags([-gamma(:,p) -(1-beta(:,p)) -alpha(:,p)], -1:1, N+1, N+1);
 A(1,2)=alpha_p(1,p);  A(1,1)=-(1+beta_p(1,p));
 B(1,2)=-alpha_p(1,p); B(1,1)=-(1-beta_pp(1,p));
 %
 %%%%% Compute coefficient of Upper BC %%%%%
 %
 eubc;
 lambda=beta(N+1,p)+dy_eta(p)*2*alpha(N+1,p)*(r(p));
 gamma_p=gamma(N+1,p)+alpha(N+1,p);
 A(N+1,N+1)=1+lambda;
 A(N+1,N)=-gamma_p;
```

```
B(N+1,N+1)=(1-lambda);
B(N+1,N)=gamma_p;
B(N+1,N+2)=1;
U(N+2,p)=4*alpha(N+1,p)*dy_eta(p)*(s(p));
U(1:N+1,p+1)=(A\B)*U(1:N+2,p);
end;
```

F.   LOWER BOUNDARY CONDITION

```
% Filename : elbc.m
% Title : Lower Boundary Conditions
% Revision No. : R1.0
% Date of Last Revision : 10 Mar 95
% Comments :
%          This program formulates the equations for the
%          impedance boundary conditions imposed on the irregular
%          lower boundary. Impedance boundary conditions relates
%          the tangential components of electric and magnetic
%          fields at the interface of two media.
%          The surface impedance is determined from the
%          intrinsic impedance of the medium by considering
%          plane wave reflections from the interface.
%
% Input Variables :
%          dx_xi              : 1st order x-derivative w.r.t. xi
%          dy_xi              : 1st order y-derivative w.r.t. xi
%          dy_eta             : 1st order y-derivative w.r.t. eta
%          alpha              : coefficient for U(p,q+1) term
%          gamma              : coefficient for U(p,q-1) term
%
% Output Variables :
%          alpha_p            : coefficient for U(p,1) term
%          beta_p             : coefficient "(1+beta_P)" for U(p,0) term
%          beta_pp            : coefficient "(1-beta_pp)" for U(p-1,0) term
%
% Associated Matlab Files :
%          Called by          : epde
%          Subroutines        : none
%
% Associated Functions       : none
%
temp2=sqrt(dx_xi(1,1:M).^2+dy_xi(1,1:M).^2);
ct=dx_xi(1,1:M)./temp2;     % cos(theta)
st=dy_xi(1,1:M)./temp2;     % sin(theta)
c1=-1j*ko*(n^2.*delta_v - st);
alpha_p=alpha(1,:)+gamma(1,:);
temp3=2.*gamma(1,:).*dy_eta(1,:).*ct;
beta_p=beta(1,:)-temp3.*(c1-2*st./dx_xi(1,1:M));
beta_pp=beta(1,:)-temp3.*(c1+2*st./dx_xi(1,1:M));
```

G.   UPPER BOUNDARY CONDITION

```
% Filename : eubc.m
% Title : Upper Boundary Conditions
% Revision No. : R1.0
% Date of Last Revision : 10 Mar 95
% Comments :
%          This program formulates the equations for the upper
%          boundary conditions at the tropospheric boundary.
%          To truncate the computational domain at the upper
%          boundary, a point high enough where the atmosphere
%          is homogeneous is considered.
%
% Input Variables :
%          dx_xi          : 1st order x-derivative w.r.t. xi
%          dy_xi          : 1st order y-derivative w.r.t. xi
%          dy_eta         : 1st order y-derivative w.r.t. eta
%          alpha          : coefficient for U(p,q+1) term
%          gamma          : coefficient for U(p,q-1) term
%
% Output Variables :
%          s              : coefficient for U(p,1) term
%
% Associated Matlab Files :
%          Called by      : epde
%          Subroutines    : none
%
% Associated Functions   : fresnel
%
tempA=0; tempB=0; tempC=0;
x=(xphy(p+1)+xphy(p))/2; % x(p-1/2)
xd=(xphy(p+1)-xphy(p))/2;            % x(p-1/2)-x(p-1)
for i=N+2:round(ytop/ydel+1);
 j=i-N-1;
 temp4(j)=fresnel(sqrt(ko/(pi*(x-xin(1)))).*(yinit(i)-yinit(N+1)));
 temp5(j)=fresnel(sqrt(ko/(pi*(x-xin(1)))).*(yinit(i-1)-yinit(N+1)));
 tempA=tempA+(Hz(i,1)-Hz(i-1,1))/ydel.*(temp4(j)-temp5(j));
end;
%
%%%%% Compute the U(N+1,p-1) term in s(p) %%%%%
%
tempA=sqrt(2j)*tempA;
tempC=sqrt(8j*ko/pi)*U(N+1,p)/sqrt(xd);
if p==1;
 s(p)=tempA+tempC;
else;
 temp6=sqrt(x-xphy(2:p))+sqrt(x-xphy(1:p-1));
 tempB=sum((U(N+1,2:p)-U(N+1,1:p-1))./temp6);
 s(p)=tempA-sqrt(8j*ko/pi)*tempB+tempC;
end;
```

H.   FRESNEL INTEGRAL FUNCTION

```
% Filename : fresnel.m
% Title : The Fresnel Integral Function
% Revision No. : R1.0
% Date of Last Revision : 10 Mar 95
% Comments :
%
% Input Variables :
%
% Output Variables :
%
% Associated Matlab Files :
%
% Associated Functions :
%
function F=fresnel(limits);
interval=0.001;
if limits==0;
  F=0;
elseif limits < 0;
  limits=-1*limits;
  tau=0:interval:limits;
  tau=-1.*tau;
  integral=exp(-1j*pi/2*(tau.*tau));
  F=trapz(tau,integral);
else
  tau=0:interval:limits;
  integral=exp(-1j*pi/2*(tau.*tau));
  F=trapz(tau,integral);
end;
```

I.   INPUT DATA FILE FOR PROPAGATION OVER PEC PLANE

```
% Filename : pec.m
% Title : Input Data File
% Revision No. : R1.0
% Date of Last Revision : 10 Mar 95
% Comments :
%        This is the input data file for computing the Parabolic
%        Equation Solution of Radiowave Propagation in an
%        Inhomogenous Atmosphere and Over Irregular Terrain.
%        It contains the frequency of operation, the x and y
%        discretization size, x- and y-coordinates of the ground
%        plane domain, and the upper boundary.
%        It also contains the surface impedance (Note : surface
%        impedance = 0 for PEC).
%
% Input Variables : none
%
```

72

```
% Output Variables :
%       xphy            : x-coordinate of physical domain
%       yphy            : y-coordinate of physical domain
%       wavelength      : wavelength (frequency/3e8)
%
% Associated Matlab Files :
%       Called by       : main
%       Subroutines     : none
%
% Associated Functions   : none
%
freq=300e6;                     % frequency of operation
wavelength=3e8/freq;            % wavelength
ko=2*pi*freq/3e8;           % free space wave number
xdel=0.1*wavelength;            % size of delta-x
ydel=0.1*wavelength;            % size of delta-y
%
%%%%% Define Ground Plane Coordinates %%%%%
%
xin(1)=5*wavelength; yin(1)=0;
xin(2)=15*wavelength; yin(2)=0;
yup=20*wavelength;              % y-upper boundary
ytop=5*wavelength+yup;          % troposphere boundary (@ infinity)
x0=0; y0=0;                     % position of transmitter
%
%%%%% Define Surface Impedance %%%%%
%
delta_v=0;                      % surface impedance (PEC)
```

J.   INPUT DATA FILE FOR PROPAGATION OVER PEC KNIFE-EDGE

```
% Filename : kpec.m
% Title : Input Data File for PEC Knife Edge
% Revision No. : R1.0
% Date of Last Revision : 10 Mar 95
% Comments :
%
% Input Variables : none
%
% Output Variables :
%       xphy            : x-coordinate of physical domain
%       yphy            : y-coordinate of physical domain
%       wavelength      : wavelength (frequency/3e8)
%
% Associated Matlab Files :
%       Called by       : main
%       Subroutines     : none
%
% Associated Functions   : none
%
```

```
freq=300e6;                         % frequency of operation
wavelength=3e8/freq;                % wavelength
ko=2*pi*freq/3e8;               % free space wave number
xdel=0.1*wavelength;                % size of delta-x
ydel=0.1*wavelength;                % size of delta-y
%
%%%%% Define Ground Plane Coordinates %%%%%
%
xin(1)=5*wavelength; yin(1)=0;
xin(2)=9.9*wavelength; yin(2)=0;
xin(3)=10*wavelength; yin(3)=2*wavelength;
xin(4)=10.1*wavelength; yin(4)=2*wavelength;
xin(5)=10.2*wavelength;yin(5)=0;
xin(6)=30*wavelength; yin(6)=0;
yup=22*wavelength;                  % y-upper boundary
ytop=5*wavelength+yup;              % troposphere boundary (@ infinity)
x0=0; y0=0;                         % position of transmitter
%
%%%%% Define Surface Impedance %%%%%
%
delta_v=0;                          % surface impedance (PEC)
```

K.   INPUT DATA FILE FOR PROPAGATION OVER CIRCULAR BOSS IN A PEC PLANE

```
% Filename : boss.m
% Title : Input Data File for Semi-Circular Boss over PEC Plane
% Revision No. : R1.0
% Date of Last Revision : 10 Mar 95
% Comments :
%
% Input Variables : none
%
% Output Variables :
%       xphy            : x-coordinate of physical domain
%       yphy            : y-coordinate of physical domain
%       wavelength      : wavelength (frequency/3e8)
%
% Associated Matlab Files :
%       Called by       : main
%       Subroutines     : none
%
% Associated Functions    : none
%
freq=3e6;                           % frequency of operation
wavelength=3e8/freq;                % wavelength
ko=2*pi*freq/3e8;               % free space wave number
xdel=0.01*wavelength;               % size of delta-x
ydel=0.05*wavelength;               % size of delta-y
%
```

```
%%%%% Define Ground Plane Coordinates %%%%%
%
b=0.5*wavelength;
A=wavelength; B=0.8*wavelength;
x_mid=-0.5*wavelength:0.01*wavelength:0.5*wavelength;
y_mid=sqrt(b^2-x_mid.^2);
x_fnt=-0.6*wavelength:0.01*wavelength:-0.51*wavelength;
y_fnt=zeros(size(x_fnt));
x_bk=0.51*wavelength:0.01*wavelength:wavelength;
y_bk=zeros(size(x_bk));
xin=[x_fnt x_mid x_bk];
%xin=xin+0.75*wavelength;
yin=[y_fnt y_mid y_bk];
clear x_fnt; clear x_mid; clear x_bk;
clear y_fnt; clear y_mid; clear y_bk;
yup=20*wavelength;              % y-upper boundary
ytop=5*wavelength+yup;         % troposphere boundary (@ infinity)
x0=-0.75*wavelength; y0=0.1*wavelength; % position of transmitter
%
%%%%% Define Surface Impedance %%%%%
%
delta_v=0;                     % surface impedance (PEC)
```

L.   INPUT DATA FILE FOR PROPAGATION OVER LOSSY IMPEDANCE PLANE

```
% Filename : imped.m
% Title : Input Data File for Lossy Impedance Plane
% Revision No. : R1.0
% Date of Last Revision : 10 Mar 95
% Comments :
%
% Input Variables : none
%
% Output Variables :
%       xphy            : x-coordinate of physical domain
%       yphy            : y-coordinate of physical domain
%       wavelength      : wavelength (frequency/3e8)
%
% Associated Matlab Files :
%       Called by       : main
%       Subroutines     : none
%
% Associated Functions   : none
%
freq=1e6;                       % frequency of operation
wavelength=3e8/freq;        _   % wavelength
ko=2*pi*freq/3e8;         % free space wave number
xdel=0.1*wavelength;            % size of delta-x
ydel=0.1*wavelength;           % size of delta-y
```

```
%
%%%%% Define Ground Plane Coordinates %%%%%
%
xin(1)=0.5*wavelength; yin(1)=0;
xin(2)=20*wavelength; yin(2)=0;
yup=20*wavelength;              % y-upper boundary
ytop=5*wavelength+yup;         % troposphere boundary (@ infinity)
x0=0; y0=wavelength/300; % position of transmitter
%
%%%%% Define Surface Impedance %%%%%
%
er=10;                         % relative permittivity
sigma=10e-3;                   % conductivity
sigma_r=60*wavelength*sigma;   % relative conductivity
delta_v=sqrt(1/(er-1j*sigma_r));% surface impedance (vertical pol)
```

M.   INPUT DATA FILE FOR PROPAGATION OVER LOSSY GAUSSIAN HILL

```
% Filename : gauss.m
% Title : Input Data File for Lossy Gaussian Hill
% Revision No. : R1.0
% Date of Last Revision : 10 Mar 95
% Comments :
%
% Input Variables : none
%
% Output Variables :
%       xphy           : x-coordinate of physical domain
%       yphy           : y-coordinate of physical domain
%       wavelength     : wavelength (frequency/3e8)
%
% Associated Matlab Files :
%       Called by      : main
%       Subroutines    : none
%
% Associated Functions   : none
%
freq=1e6;                      % frequency of operation
wavelength=3e8/freq;           % wavelength
ko=2*pi*freq/3e8;        % free space wave number
xdel=0.1/3*wavelength;         % size of delta-x
ydel=0.1*wavelength;           % size of delta-y
%
%%%%% Define Ground Plane Coordinates %%%%%
%
Ht=1000; c=5000; w=3000;       % constants for gaussian hill
xin=2000:xdel:24*wavelength;% x-coordinate
yin=Ht.*exp(-9.*(((xin-c)./w).^2)); % y-coordinate
yup=30*wavelength;             % y-upper boundary
ytop=5*wavelength+yup;         % troposphere boundary (@ infinity)
```

```
x0=0; y0=wavelength/100; % position of transmitter
%
%%%%% Define Surface Impedance %%%%%
%
er=10;                            % relative permittivity
sigma=10e-3;                      % conductivity
sigma_r=60*wavelength*sigma;      % relative conductivity
delta_v=sqrt(1/(er-1j*sigma_r));% surface impedance (vertical pol)
```

N.   INPUT DATA FILE FOR PROPAGATION OVER PEC ISOSCELES HILL

```
% Filename : isos.m
% Title : Input Data File for PEC Isosceles Hill
% Revision No. : R1.0
% Date of Last Revision : 10 Mar 95
% Comments :
%
% Input Variables : none
%
% Output Variables :
%       xphy            : x-coordinate of physical domain
%       yphy            : y-coordinate of physical domain
%       wavelength      : wavelength (frequency/3e8)
%
% Associated Matlab Files :
%       Called by       : main
%       Subroutines     : none
%
% Associated Functions   : none
%
freq=9.6e9;                      % frequency of operation
wavelength=3e8/freq;             % wavelength
ko=2*pi*freq/3e8;         % free space wave number
xdel=0.08*wavelength;            % size of delta-x
ydel=0.08*wavelength;            % size of delta-y
%
%%%%% Define Ground Plane Coordinates %%%%%
%
xin(1)=5.12*wavelength; yin(1)=0;
xin(2)=10.24*wavelength; yin(2)=0;
xin(3)=20.32*wavelength; yin(3)=1.232*wavelength;
xin(4)=30.4*wavelength; yin(4)=0;
xin(5)=64*wavelength; yin(5)=0;
yup=20*wavelength;               % y-upper boundary
ytop=5*wavelength+yup;           % troposphere boundary (@ infinity)
x0=0; y0=0;                      % position of transmitter
%
%%%%% Define Surface Impedance %%%%%
%
delta_v=0;                       % surface impedance (PEC)
```

77

O. INPUT DATA FILE FOR PROPAGATION OVER PEC CLIFF

```
% Filename : cliff.m
% Title : Input Data File for PEC Cliff
% Revision No. : R1.0
% Date of Last Revision : 10 Mar  95
% Comments :
%
% Input Variables : none
%
% Output Variables :
%       xphy            : x-coordinate of physical domain
%       yphy            : y-coordinate of physical domain
%       wavelength      : wavelength (frequency/3e8)
%
% Associated Matlab Files :
%       Called by       : main
%       Subroutines     : none
%
% Associated Functions   : none
%
freq=9.6e9;                         % frequency of operation
wavelength=3e8/freq;                % wavelength
ko=2*pi*freq/3e8;               % free space wave number
xdel=0.08*wavelength;               % size of delta-x
ydel=0.08*wavelength;               % size of delta-y
%
%%%%% Define Ground Plane Coordinates %%%%%
%
xin(1)=5.12*wavelength; yin(1)=1.0464*wavelength;
xin(2)=10.24*wavelength; yin(2)=1.0464*wavelength;
xin(3)=10.34*wavelength; yin(3)=0;
xin(4)=80*wavelength; yin(4)=0;
yup=21*wavelength;                  % y-upper boundary
ytop=5*wavelength+yup;              % troposphere boundary (@ infinity)
x0=0; y0=yin(1);            % position of transmitter
%
%%%%% Define Surface Impedance %%%%%
%
delta_v=0;                          % surface impedance (PEC)
```

P. INPUT DATA FILE FOR PROPAGATION OVER DIELECTRIC COATED CLIFF

```
% Filename : diele.m
% Title : Input Data File for Dielectric coated Cliff
% Revision No. : R1.0
% Date of Last Revision : 10 Mar 95
% Comments :
```

```
%
% Input Variables : none
%
% Output Variables :
%         xphy            : x-coordinate of physical domain
%         yphy            : y-coordinate of physical domain
%         wavelength      : wavelength (frequency/3e8)
%
% Associated Matlab Files :
%         Called by       : main
%         Subroutines     : none
%
% Associated Functions    : none
%
freq=9.6e9;                         % frequency of operation
wavelength=3e8/freq;                % wavelength
ko=2*pi*freq/3e8;               % free space wave number
xdel=0.08*wavelength;               % size of delta-x
ydel=0.08*wavelength;               % size of delta-y
%
%%%%% Define Ground Plane Coordinates %%%%%
%
xin(1)=0.5*wavelength; yin(1)=1.0464*wavelength;
xin(2)=10.24*wavelength; yin(2)=1.0464*wavelength;
xin(3)=10.34*wavelength; yin(3)=0;
xin(4)=80*wavelength; yin(4)=0;
yup=21*wavelength;                  % y-upper boundary
ytop=5*wavelength+yup;              % troposphere boundary (@ infinity)
x0=0; y0=yin(1);            % position of transmitter
%
%%%%% Define Surface Impedance %%%%%
%
delta_v=0.171j;                     % surface impedance
```

Q.   INPUT DATA FILE FOR PROPAGATION OVER MIXED PATH

```
% Filename : mix.m
% Title : Input Data File for Land-Sea-Land
% Revision No. : R1.0
% Date of Last Revision : 10 Mar 95
% Comments :
%
% Input Variables : none
%
% Output Variables :
%         xphy            : x-coordinate of physical domain
%         yphy            : y-coordinate of physical domain
%         wavelength      : wavelength (frequency/3e8)
%
% Associated Matlab Files :
```

```
%        Called by       : main
%        Subroutines     : none
%
% Associated Functions   : none
%
freq=59.7e6;
wavelength=3e8/freq;                    % wavelength
ko=2*pi*freq/3e8;              % Free space wave number
ydel=0.2;                              % y-delta size
%
%%%%% Define Ground Plane Coordinates %%%%%
%
xin(1)=40000; yin(1)=0; xdel(1)=100; impz(1)=sqrt(1/(15-9.045j));
xin(2)=47000; yin(2)=0; xdel(2)=10; impz(2)=sqrt(1/(80-1206j));
xin(3)=50000; yin(3)=0; xdel(3)=1; impz(3)=sqrt(1/(15-9.045j));
xin(4)=52000; yin(4)=0; xdel(4)=100; impz(4)=sqrt(1/(15-9.045j));
xin(5)=60000; yin(5)=0; impz(5)=sqrt(1/(15-9.045j));
yup=10;
ytop=5*wavelength+yup;
x0=0; y0=5;
```

R.   INPUT DATA FILE FOR PROPAGATION OVER LOSSY VALLEY

```
% Filename : valley.m
% Title : Input Data File for Valley
% Revision No. : R0.2
% Date of Last Revision : 20 Feb 95
% Comments :
%
% Input Variables : none
%
% Output Variables :
%        xphy            : x-coordinate of physical domain
%        yphy            : y-coordinate of physical domain
%        wavelength      : wavelength (frequency/3e8)
%
% Associated Matlab Files :
%        Called by       : main
%        Subroutines     : none
%
% Associated Functions   : none
%
freq=10e6;                              % frequency of operation
wavelength=3e8/freq;                    % wavelength
ko=2*pi*freq/3e8;              % free space wave number
ydel=0.1*wavelength;                   % size of delta-y
%
%%%%% Define Ground Plane Coordinates %%%%%
%
xin(1)=28000; yin(1)=100; xdel(1)=300;
```

```
xin(2)=30000; yin(2)=100; xdel(2)=3;
xin(3)=31000; yin(3)=0;  xdel(3)=3;
xin(4)=32000; yin(4)=0;  xdel(4)=3;
xin(5)=33000; yin(5)=100; xdel(5)=3;
xin(6)=35000; yin(6)=100; xdel(6)=30; ·
xin(7)=50000; yin(7)=100;
yup=50+yin(1);
ytop=5*wavelength+yup;
x0=0; y0=yin(1);
%
%%%%% Define Surface Impedance %%%%%
%
er=4;                          % relative permittivity
sigma=1e-3;                    % conductivity
sigma_r=60*wavelength*sigma;   % relative conductivity
delta_v=sqrt(1/(er-1j*sigma_r));% surface impedance (vertical pol)
```

LIST OF REFERENCES

1. S. W. Marcus, "A Hybrid (Finite Difference - Surface Green's Function) Method for Computing Transmission Losses in an Inhomogeneous Atmosphere and Over Irregular Terrain," *IEEE Trans. Propagat.*, Vol 40, No. 12, pp. 1451-1458, Dec. 1992.

2. R. Janaswamy, "Efficient Parabolic Equation Solution of Radiowave Propagation in an Inhomogeneous Atmosphere and Over Irregular Terrain : Formulation," Tech. Rep. NPS-EC-94-015, Naval Postgraduate School, Monterey, California, Nov. 1994.

3. T. B. A. Senior, "Impedance Boundary Conditions for Imperfectly Conducting Surfaces," *Appl. Sci. Res.*, Sec. B, Vol. 8, pp. 418-436, 1960.

4. C. A. Balanis, *Advanced Engineering Electromagnetics*, John Wiley & Sons, New York, pp. 180-193, 1989.

5. F. B. Jensen, et al., *Computational Ocean Acoustics*, AIP Press, New York, pp. 343-352, 1993.

6. M. Abramowitz and I. A. Stegun, *Handbook of Mathematical Functions*, Dover, New York, pp. 321-323, 1965.

7. J. F. Thompson, Z. U. A. Warsi, and C. W. Mastin, *Numerical Grid Generation*, North Holland, New York, pp. 117-133, 1985.

8. G. D. Smith, *Numerical Solution of Partial Differential Equations : Finite Difference Methods*, Oxford University Press, New York, pp. 19-24, 1985.

9. R. Janaswamy, "A Fredholm Integral Equation Method for Propagation Over Small Terrain Irregularities," *IEEE Trans. Antennas Propagat.*, Vol. 40, No. 11, pp. 1416-1422, Nov. 1992.

10. Z. Wu, T. S. M. Maclean, D. J. Bagwell, and M. J. Mehler, "Propagation Over an Inhomogeneous Irregular Surface," *Radio Sci.*, Vol. 23, pp. 33-40, Jan.-Feb. 1988.

11. R. Janaswamy, "Application of the Measured Equation of Invariance to Wave Propagation over Irregular, Inhomogeneous Terrain" Tech. Rep. NPS-EC-93-018, Naval Postgraduate School, Monterey, California, Oct. 1993.

12. R. H. Ott, " A New Method for Predicting HF Ground Wave Attenuation Over Inhomogeneous, Irregular Terrain," Inst. for Telecommun. Sci., Office of Telecommun., U.S. Dep. Commerce, Boulder, Colorado 80302, OT/ITS Res. Rep. 7, 1971a.

13. G. Millington, "Ground Wave Propagation Over an Inhomogeneous Smooth Earth," *Proc. IEE (London), Part III*, Vol. 96, pp. 53, Jan. 1949.

INITIAL DISTRIBUTION LIST

No. of Copies

1. Defense Technical Information Center   2
   Cameron Station
   Alexandria, Virginia 22304-6145

2. Library, Code 52   2
   Naval Postgraduate School
   Monterey, California 93943-5101

3. Chairman, Code EC   1
   Department of Electrical and Computer Engineering
   Naval Postgraduate School
   Monterey, California 93943-5121

4. Professor Ramakrishna Janaswamy, Code EC/Js   10
   Department of Electrical and Computer Engineering
   Naval Postgraduate School
   Monterey, California 93943-5121

5. Professor Lawrence J. Ziomek, Code EC/Zm   1
   Department of Electrical and Computer Engineering
   Naval Postgraduate School
   Monterey, California 93943-5121

6. Professor Richard Adler, Code EC/Ab   1
   Department of Electrical and Computer Engineering
   Naval Postgraduate School
   Monterey, California 93943-5121

7. LCDR Gus. K. Lott, Code EC/Lt   1
   Department of Electrical and Computer Engineering
   Naval Postgraduate School
   Monterey, California 93943-5121

8. Herbert Hitney   1
   NCCOSC RDTE DIV 543
   49170 Propagation Path
   San Diego, California 92152-7385

9.   Dr. Sherman Marcus   1
        RAFAEL, Dept. 7C
        P. O. Box 2250
        Haifa, Israel

10.   Professor J. B. Andersen   1
        Center for Personkommunikation
        Aalborg University, Fr. Bajers Vej 7, Dk-9220
        Aalborg, Denmark

11.   MAJ Lee, Joo-Kiong   2
        TRC - CMPB
        CMPB Podium, Depot Road
        Singapore 0410